frontiers | Frontiers in Earth Science

TYPE Original Research
PUBLISHED 11 October 2022
DOI 10.3389/feart.2022.989478



OPEN ACCESS

EDITED BY
Thomas Gentzis,
Core Laboratories, United States

REVIEWED BY
Amr Deaf,
Assiut University, Egypt
Nader Edress,
Helwan University, Egypt
Kai Mangelsdorf,
German Research Centre for Geosciences (GFZ) Potsdam, Germany

*CORRESPONDENCE
Sebastian Grohmann,
sebastian.grohmann@emr.rwth-aachen.de

SPECIALTY SECTION
This article was submitted to Geochemistry, a section of the journal Frontiers in Earth Science

RECEIVED 08 July 2022
ACCEPTED 11 August 2022
PUBLISHED 11 October 2022

CITATION
Zhao Z, Grohmann S, Zieger L, Dai W and Littke R (2022), Evolution of organic matter quantity and quality in a warm, hypersaline, alkaline lake: The example of the Miocene Nördlinger Ries impact crater, Germany.
*Front. Earth Sci.* 10:989478.
doi: 10.3389/feart.2022.989478



# Evolution of organic matter quantity and quality in a warm, hypersaline, alkaline lake: The example of the Miocene Nördlinger Ries impact crater, Germany

Zibin Zhao, Sebastian Grohmann*, Laura Zieger, Wanyu Dai and Ralf Littke

Institute of Geology and Geochemistry of Petroleum and Coal, Energy and Mineral Resources Group (EMR), RWTH Aachen University, Aachen, Germany

The Nördlinger Ries (NR) impact crater in southern Germany contains Miocene lacustrine fine-grained post-impact sediments, which were deposited under saline, alkaline, and hydrologically closed aquatic conditions. To obtain information on the organic matter quantity, quality and environmental evolution, samples from one central (NR 1973) and one more marginal (Enkingen SUBO-18) well were analyzed by pyrolytic, organic geochemical and micro-petrographic techniques. Deposits of the marginal drilling can be linked to the thicker stratigraphic units of the well from the lake center based on total organic carbon (TOC), hydrogen index (HI) and lithology. Central deposits contain mainly hydrogen-rich type I kerogen with a mean HI of 447 mg HC/g TOC, whereas the marginal sequence contains type II-III kerogen with an average HI of 206 mg HC/g TOC. In the center, high total sulfur (TS) over TOC ratios of 1.5 on average, and $\delta^{13}C$ values of biomarkers in combination with low α-/total MTTC (α-/total methyl-trimethyltridecyl chromans ~ <0.6) and Pr/Ph ratios <0.2 suggest the prevalence of hypersaline water. Salinity only decreased during deposition of the uppermost Miocene units, when the then shallow alkaline lake turned, at least temporarily, into acidic-neutral conditions during the time of peat deposition. A similar trend, but at overall lower salinities is recorded for the marginal site. Water stratification in the center is stronger than in the marginal domain based on salinity variation. Anoxic bottom water prevailed in the whole lake, as recorded by exceptionally low Pr/Ph ratios (~<0.2), the occurrence of des-A-lupane and small pyrite framboids (<5 µm) except for the youngest layers of the Miocene lake. Autochthonous, halophilic red algae/plankton prevailed as reflected by abundant $C_{27}$ steranes, while terrestrial material and aerobic bacteria significantly contributed to the OM only in the latest stages of lake as evident from abundant vitrinite/inertinite particles, high values of diterpenes/$C_{27}$ sterane (up to 255) as well as low values of $C_{27-29}$ regular steranes/$C_{29-32}$ hopanes (<0.5). The same trend, but less well resolved, can be seen at the margin of the paleo-lake.

KEYWORDS

Nördlinger Ries, impact crater, Miocene paleo-climate, alkaline paleo-lake, hypersaline palaeo-lake

# 1 Introduction

Lacustrine post-impact sequences in impact craters are invaluable paleo-environmental archives, as the impact event creates accommodation space for continuous deposition, which is usually not affected by fluvial sediment transport from outside the crater area (Koeberl et al., 2007; Shanahan et al., 2009). An example of such a lacustrine system is the Miocene Nördlinger Ries in southern Germany, which developed from an initial, alkaline, partly hypersaline, 250 m deep lake to a shallow swampy lake at the end of its evolution (Jankowski, 1981; Arp et al., 2021). Alkaline lakes are generally characterized by high concentrations of soluble carbonate salts with high pH values (pH>9) and often a hypersaline/saline water column (Pecoraino et al., 2015; Warren, 2016; Cao et al., 2020). Alkaline lakes are not common on Earth both currently and in geological times, as compared to freshwater lacustrine systems (Lowenstein et al., 2017). Ancient alkaline sediments and sedimentary rocks have been found in e.g., the Neoarchean Tumbiana Formation (Western Australia, Stüeken et al., 2015), Cambrian Observatory Hill Formation (Officer Basin, Southgate et al., 1989), Carboniferous–Permian Fengcheng Formation (Junggar Basin, Cao et al., 2020), Jurassic Towaco Formation (Newark Basin, Stüeken et al., 2019), Lower Cretaceous in offshore Campos (Neocomian, Mohriak et al., 1990), Paleogene Hetaoyuan Formation (Nanxiang Basin, Yang et al., 2015) and Paleogene Green River Shale (the United States, Stüeken et al., 2019). Modern alkaline lakes, e.g., Nakuru, can be characterized by high pH values (pH=10.9), high salinity (63‰) and high bio-productivity (gross primary carbon production rate of 1,046 g C/($m^2$a)) because of the thriving microbial community (Hammer, 1981). Alkaline lakes exhibit extreme ecological and hydrological conditions (e.g., restricted biocommunity composition, hypersaline and alkaline water chemistry, Hammer, 1981; Pecoraino et al., 2015) and the sediments, which record important geological, environmental and geo-biological information, consequently mimic the biogeochemical and depositional evolution on ancient Earth in extreme environments as far back as Neoarchean (Cao et al., 2020; Wang et al., 2021).

The Nördlinger Ries (NR) was formed by a meteorite impact that created an almost circular shaped crater of about 20 km in diameter, which was consecutively filled with Miocene lacustrine, fine-grained post-impact sediments (Füchtbauer and von der Brelie, 1977; Rullkötter et al., 1990; Arp et al., 2014; Figure 1). As one of the best-preserved and best-known impact structures on Earth (Hörz et al., 1983; Stöffler et al., 2013), NR is characterized by a pronounced structural rim around the crater (Rullkötter et al., 1990; Figure 1). A hydrologically closed lacustrine depositional system (Rothe and Hoefs, 1977; Arp et al., 2014; Christ et al., 2018) formed after the impact, exhibiting an alkaline depositional water body for most of the time and silting up during the late Miocene (Arp et al., 2017; Stüeken et al., 2020). With the rising interests in paleo-environmental archives and post-impact sedimentation processes in general, not only the impact process itself but also the post-impact sequence in the NR became a hot spot for scientific studies lately (e.g., Stöffler et al., 2013; Arp et al., 2014; Sturm et al., 2015; Arp et al., 2017; Christ et al., 2018; Arp et al., 2019; Stüeken et al., 2020; Arp et al., 2021; Zeng et al., 2021). Accordingly, impact dating, pre-impact strata modification and evolution of crater lake chemistry were studied, mainly based on samples from a single borehole. Aside from the questions concerning the immediate response to the impact, a key question remains concerning the spatiotemporal evolution of the paleo-environment and paleo-climate (Arp et al., 2014) as recorded in the sedimentary sequence. The post-impact sediments have previously been documented to be organic matter (OM)-rich in the central crater (Rullkötter et al., 1990). The amount of soluble extract (bitumen) normalized to total organic carbon (TOC) was generally found to be much higher than expected for thermally immature sediments. This surprising fact was assumed to be controlled by the high organic-sulfur content of the kerogen in NR sediments with high atomic ratios of organic sulfur over carbon ($S_{org}/C_{org}$>0.04) (Rullkötter et al., 1990). Type I-S or type I kerogens were reported to occur in the laminite unit (Figure 2) based on the atomic hydrogen/carbon ratios (H/C>1.5) of kerogens and the rare existence of pyrite (Rullkötter et al., 1990). A special, iron-poor lake chemistry has been suggested by Jankowski (1981), which is related to the position of the NR crater in the Swabian Alb mountain range, consisting mainly of carbonates and marlstones. The depositional environment was suggested to be anoxic and saline with the presence of calcite, dolomite and occasional gypsum, various extractable organic-sulfur compounds as well as low ratios of pristane over phytane (Pr/Ph) in the lower part of the fine post-impact sequence in the central domain (Rullkötter et al., 1990). An array of inorganic geochemical investigations (e.g., carbon, oxygen and strontium isotopes of carbonates, bulk rock element composition) was carried out leading to partly differing opinions concerning the water chemistry evolution and environmental conditions (e.g., water salinity and stratification) prevailing within the paleo-lake (Arp et al., 2014).

Previous molecular organic geochemistry studies focused on either selected, isolated extractable compounds or on a wider range of compounds studied, however, on just a few samples (<5 samples) (Rullkötter et al., 1990; Barakat and Rullkötter, 1994a; Barakat et al., 1994; Barakat and Rullkötter, 1994b; Barakat and Rullkötter, 1995a; Barakat and Rullkötter, 1995b;

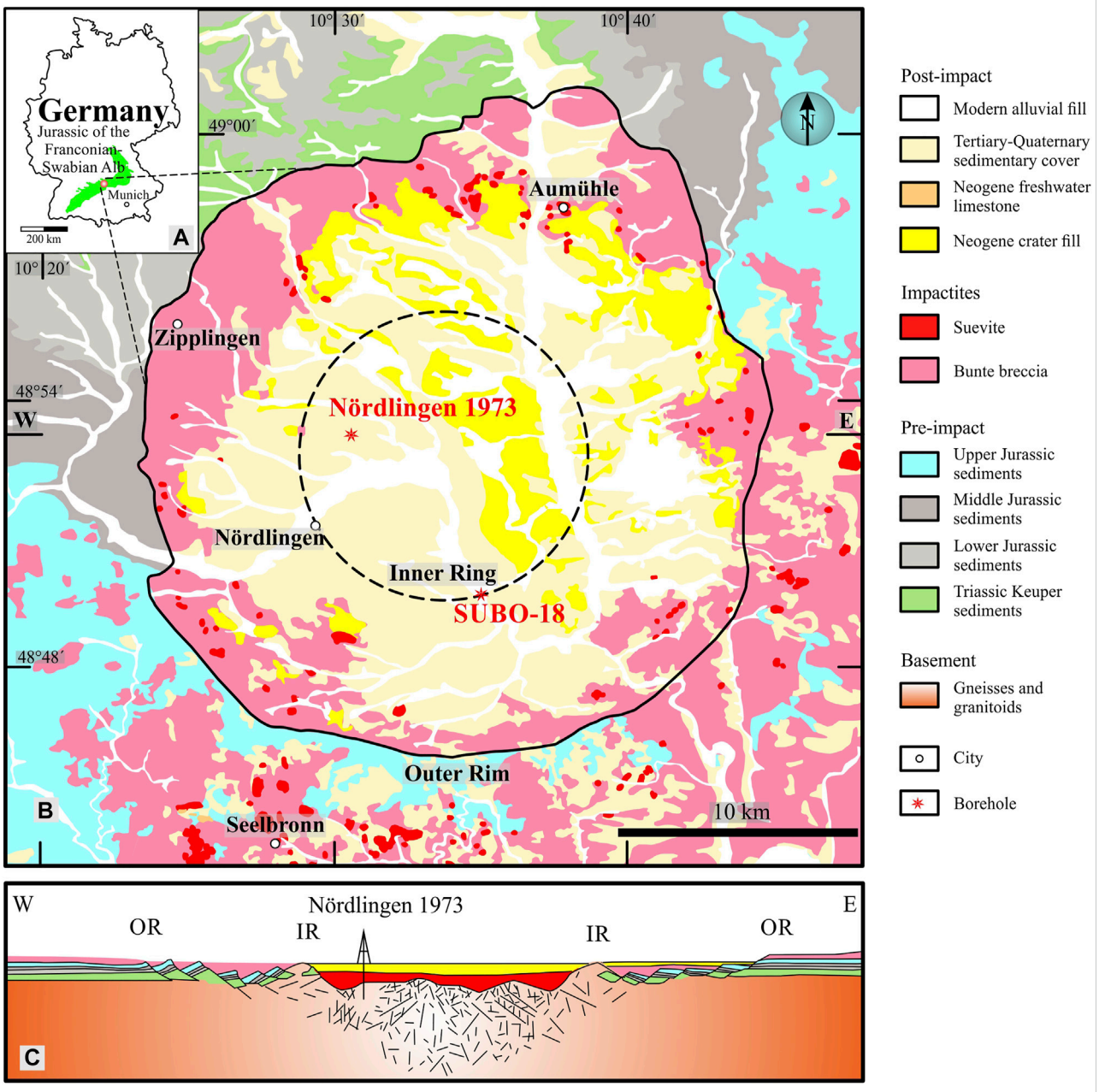


FIGURE 1
Geological map of the study area in **(A)** southern Germany showing **(B)** the Nördlinger Ries impact crater with the drilling location NR-1973 (central crater) and SUBO-18 (marginal crater) relative to the inner ring (modified after Erickson et al., 2017), as well as **(C)** an east-west seismic cross section of the crater.

Barakat and Rullkötter, 1997; Barakat and Rullkötter, 1999; Barakat et al., 2012; Barakat et al., 2013; Arp et al., 2014). Accordingly, the goal of this study is to provide a comprehensive molecular geochemical investigation on a large set of samples covering both the central and marginal lake facies from the basal deep water laminites to the upper coal-bearing sediments. This will provide new data for 1) confirming or improving current stratigraphic correlations between the central and marginal site, 2) recording climatic, depositional as well as ecological evolution of the lake system and 3) implications for water chemistry evolution and OM vulcanization in hypersaline, alkaline lakes based on bulk and extractable molecular organic geochemical and petrological features.

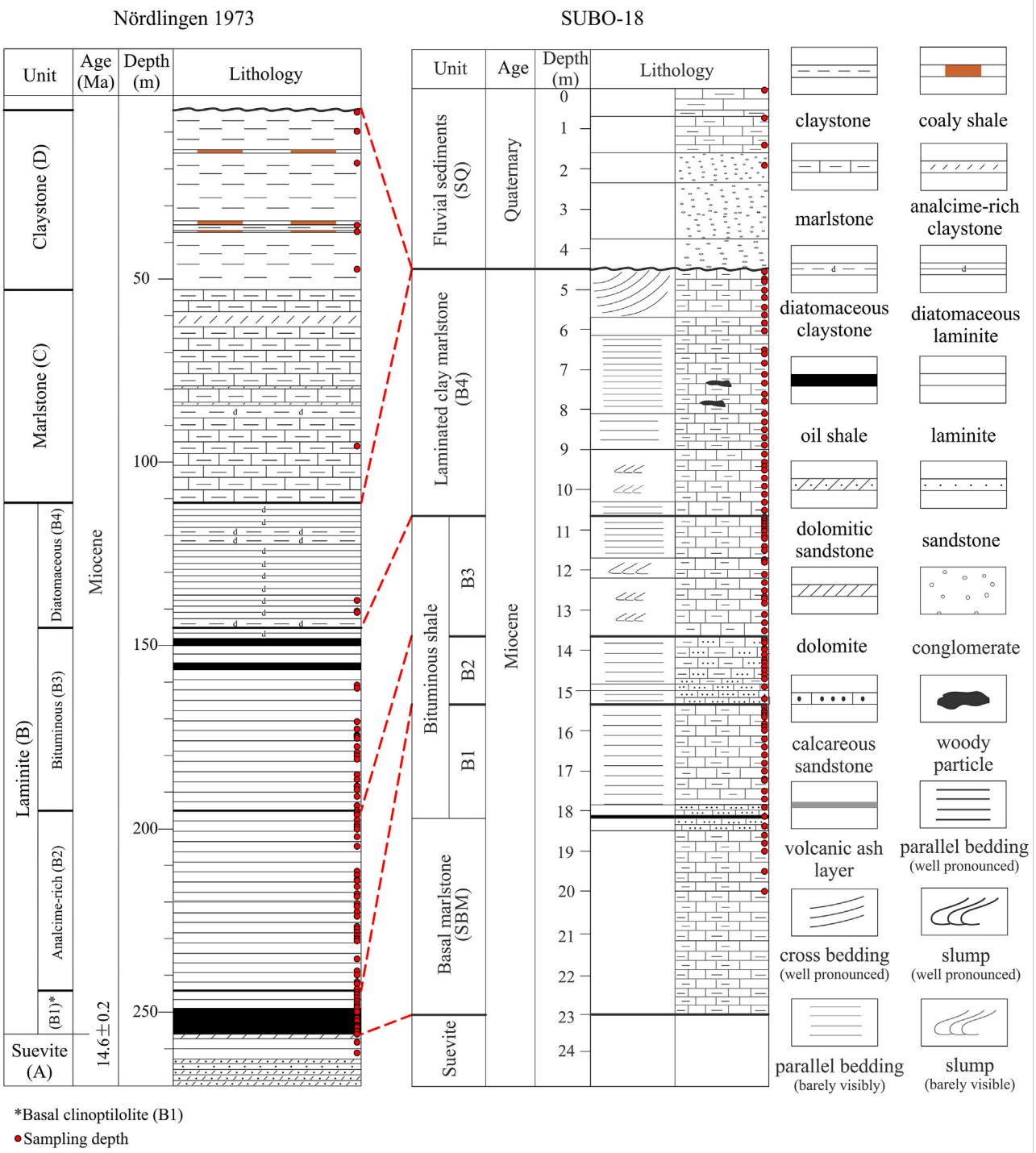


FIGURE 2
Lithological columns of the studied Nördlinger Ries boreholes. The lithology of the central borehole Nördlingen 1973 is based on Füchtbauer and von der Brelie (1977) and Rullkötter et al. (1990), whereas the presented column of the marginal borehole SUBO-18 was partly newly logged by the authors in this study with the main lithology boundaries based on Arp et al. (2014). Units C and D are missing in borehole SUBO-18. Note that the depth scale is different for both boreholes.

## 2 Geological setting

The NR is a mid-sized, almost circular-shaped Miocene lacustrine basin, with a lateral extension of 20 and 24 km in east-west and north-south orientation, respectively. It is situated in western Bavaria 100 km northwest from Munich in the southern German scarplands (Figure 1) (Rullkötter et al., 1990; Arp et al., 2019). The crater lake developed at 14.6 ± 0.2 Ma (Buchner et al., 2010) following a meteorite impact, separating the Swabian and Franconian Albs (Arp et al., 2019). The impact penetrated 600–800 m of Mesozoic to Cenozoic sedimentary rocks, covering a Variscan basement which is constituted by amphibolite, granite and gneiss (Hüttner and Schmidt-Kaler, 1999), without any coherent impact melt sheet reported at the present (Arp et al., 2019). The penetrated Mesozoic–Cenozoic sediments include Triassic shales, sandstones and evaporites (e.g., gypsum and anhydrite in Keuper succession), Jurassic carbonates, marlstones, shales and sandstones, and a thin section of unconsolidated Neogene sediments on the surface (Mujal and Schoch, 2020). The NR is composed of a central crater, an inner ring and a marginal megablock zone diverging from the inside out of the current day geometry (Pohl et al., 1977). Surrounded by the inner ring, the central crater is filled with Miocene post-impact sediments having a surface diameter of 12 km and a maximum 800 m thickness (Jankowski, 1977; Stöffler and Wu, 1977). The inner ring belt consists of crystalline basement blocks having a width of 1–2 km, and is geographically exposed in the western/southern part of the Ries plain, but buried by lake sediments in the north (Arp et al., 2019). Parautochthonous blocks that downfaulted and slumped into the cavity during crater modification formed the megablock zone (Arp et al., 2019), corresponding to the terrace zone in impact crater structures elsewhere (Melosh and Ivanov, 1999; Sturm et al., 2015). The ejected impact rocks form an "outer rim" embracing the whole impact structure as the outer boundary, which has prevented fluvial input from domains surrounding the crater lake (Rullkötter et al., 1990). The blocking effect of the "outer rim" resulted in a closed lacustrine environment, in which the sediments mainly originated from weathering products of rocks inside the outer rim (Arp et al., 2014).

Three Miocene post-impact lithofacies are recognized in the crater, i.e., marginal fluvio-deltaic siliciclastics and carbonates, marginal carbonates, and a basinal argillaceous sequence (Arp et al., 2014). The basinal argillaceous sequence is subdivided into four sections (Figure 2), composed from bottom to top of the basal reworked suevite unit A, the laminite unit B, the marlstone unit C and the claystone interbedded with lignite unit D, as revealed by the near center borehole Nördlingen-1973 (NR-1973) (Füchtbauer and von der Brelie, 1977; Jankowski, 1981; Rullkötter et al., 1990). Four subunits are further defined for unit B, i.e., clinoptilolite subunit B1, analcime subunit B2, bituminous subunit B3 and diatomaceous subunit B4, based on their OM content, zeolite species and palynological features (Rullkötter et al., 1990). It was assumed that the deposition of the post-impact sediments took 1.2 to 2 Ma after the formation of the crater about 14.6 Ma ago (Montano et al., 2021). Approximately 100 m of the latest Miocene lake sediments were eroded during the Pliocene and Pleistocene (Füchtbauer and von der Brelie, 1977; Bader and Schmidt-Kaler, 1990); the marginal carbonate and siliciclastics lithofacies, which are exposed near the crater rim, are probably time-equivalently sediments to the eroded central sediments (Arp et al., 2014). The marginal carbonates, composed of dolomitic algal bioherms, palustrine limestones, carbonate sands and travertine, can reach a thickness of 50 m (Wolf and Füchtbauer, 1976; Riding, 1979).

SUBO-18 (Enkingen) only encountered around 23 m post-impact sediments overlying the suevite base (Figure 2). The sedimentary succession was divided into four lithological units: 1) sandstone bearing basal marlstone (bottom–18.3 m), 2) bituminous shale (18.3–10.65 m), 3) laminated clayey marlstone (10.65–4.5 m), 4) fluvial gravel, clay and silt (4.5–0 m). The latest unit (4.5–0 m) was deposited during the Quaternary (Arp et al., 2014), while the other three units were attributed to Miocene age, which were assumed to be equivalent either to upper unit B–lower unit C (Arp et al., 2014) or units B1–B3 in the NR-1973 (Arp et al., 2021). Units C and D, in any case, are not present in the SUBO-18 borehole.

## 3 Samples and methods

### 3.1 Samples

A total of 176 post-impact lacustrine shale samples were acquired from the NR-1973 (80) and SUBO-18 (96) wells, drilled in the central crater and the inner ring periphery of the Nördlinger Ries, respectively (Figures 1, 2). For the NR-1973 well, cores were sampled over a range of 261 m with the focus and the most dense and regular sampling (at least one sample per meter) in the organic-rich sections from about 140 to 260 m, considering all the Miocene lacustrine sedimentary units (6 samples from unit D, 1 sample from unit C, 70 samples from unit B and 3 samples from unit A) in the Ries impact crater (Figure 2). From the SUBO-18 well, samples were taken at last every 20 cm (from surface to ca. 20 m) and locations with exceptionally dark intervals were sampled in even smaller intervals. For bulk geochemical (total organic carbon (TOC), total inorganic carbon (TIC), total sulfur (TS) and Rock-Eval pyrolysis), as well as molecular geochemical (gas chromatography (GC-FID) and gas chromatography-mass spectroscopy (GC-MS)) measurements, rock samples were pulverized using an agate mortar and afterwards homogenized and dried at 50°C overnight in the oven. Sample selection for molecular organic geochemical and organic petrological analyses was based on TOC contents and stratigraphy.

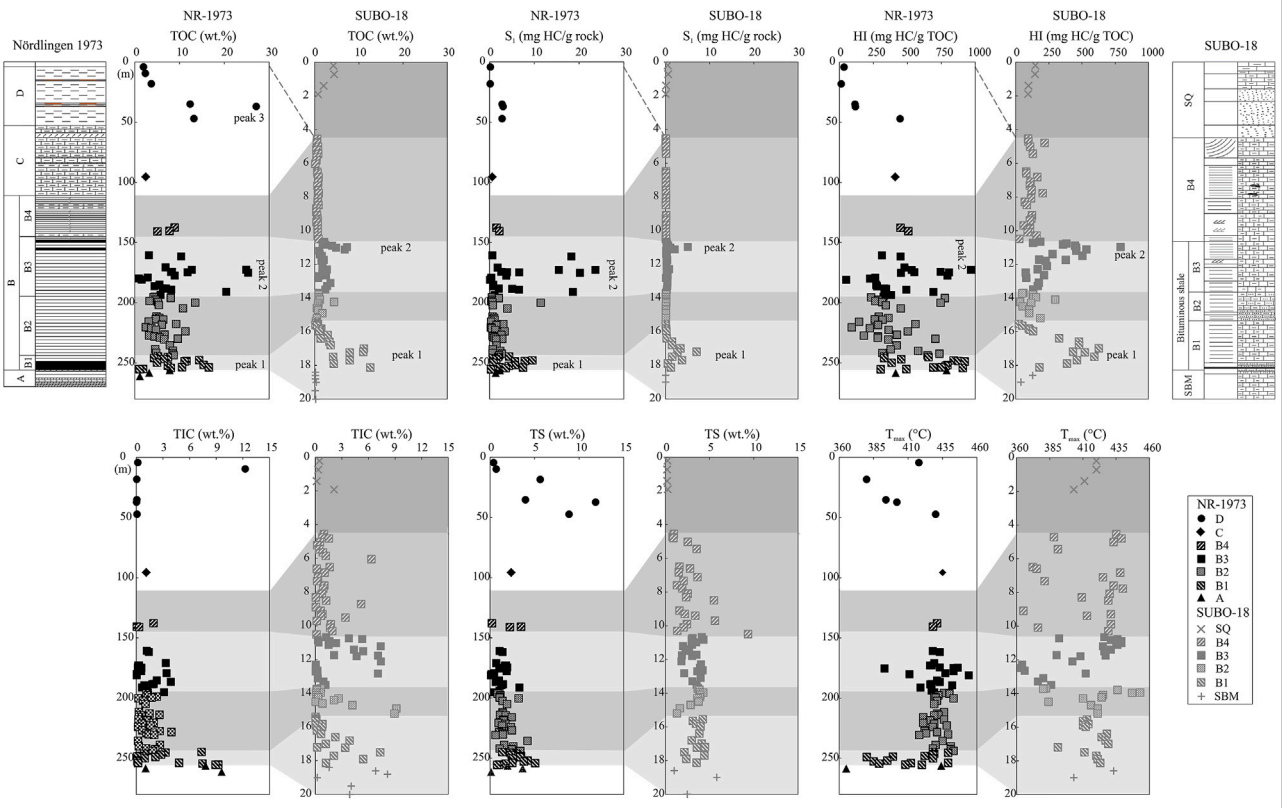


FIGURE 3
Bulk elemental data (TOC=total organic carbon content, TIC=total inorganic carbon content, TS=total sulfur content) and Rock-Eval indices ($S_1$= thermovaporized hydrocarbons, $T_{max}$= temperature of maximum pyrolytic hydrocarbon generation, HI= hydrogen index) for the post-impact sediments in the NR-1973 and SUBO-18. See Figure 2 for stratigraphic units.

## 3.2 Elemental analysis

TOC and TIC contents of all samples from both boreholes were measured using an Elementar LiquiTOC II analyzer. Approximately 100 mg of unacidified powder was combusted at temperatures of 550°C (TOC) and 1,100°C (TIC) in the presence of oxygen. Details on the experimental method are summarized in Zhao et al. (2020). TS measurements were conducted on 158 samples (there was no more sample material for the remaining samples) with a Leco S200 sulfur analyzer for which detection limit and precision are 20 ppm and <5%. Details of the procedure are explained in Prinz et al. (2017).

## 3.3 Rock-Eval pyrolysis

Rock-Eval pyrolysis was conducted on 155 samples having TOC values above 0.5% utilizing a Rock-Eval six Pyrolyzer, following the experimental and interpretative methods documented by Espitalié et al. (1985) and Behar et al. (2001) for acquiring qualitative information on the OM within the sediments. Around 50 mg of each pulverized sample was weighed for measurement. Thermovaporized hydrocarbons ($S_1$, mg HC/g rock) were recorded during the 300°C isothermal stage and thermally cracked hydrocarbons ($S_2$, mg HC/g rock) were recorded during heating between 300 and 650°C. Generated hydrocarbons were detected by a flame ionization detector (FID). $T_{max}$ corresponds to the calibrated temperature of maximum pyrolytic hydrocarbon generation.

## 3.4 Molecular organic geochemistry

Selected samples from the NR-1973 well were prepared for glycerol dialkyl glycerol tetraether (GDGT) measurements. Only one of the samples turned out to contain valuable amounts of GDGTs (18/691, unit D). The methodology and formula for water temperature calculation are given in the Supplementary Appendix A1.

Solvent extraction was performed on 36 samples showing among the highest TOC and TS values with a Thermo DIONEX

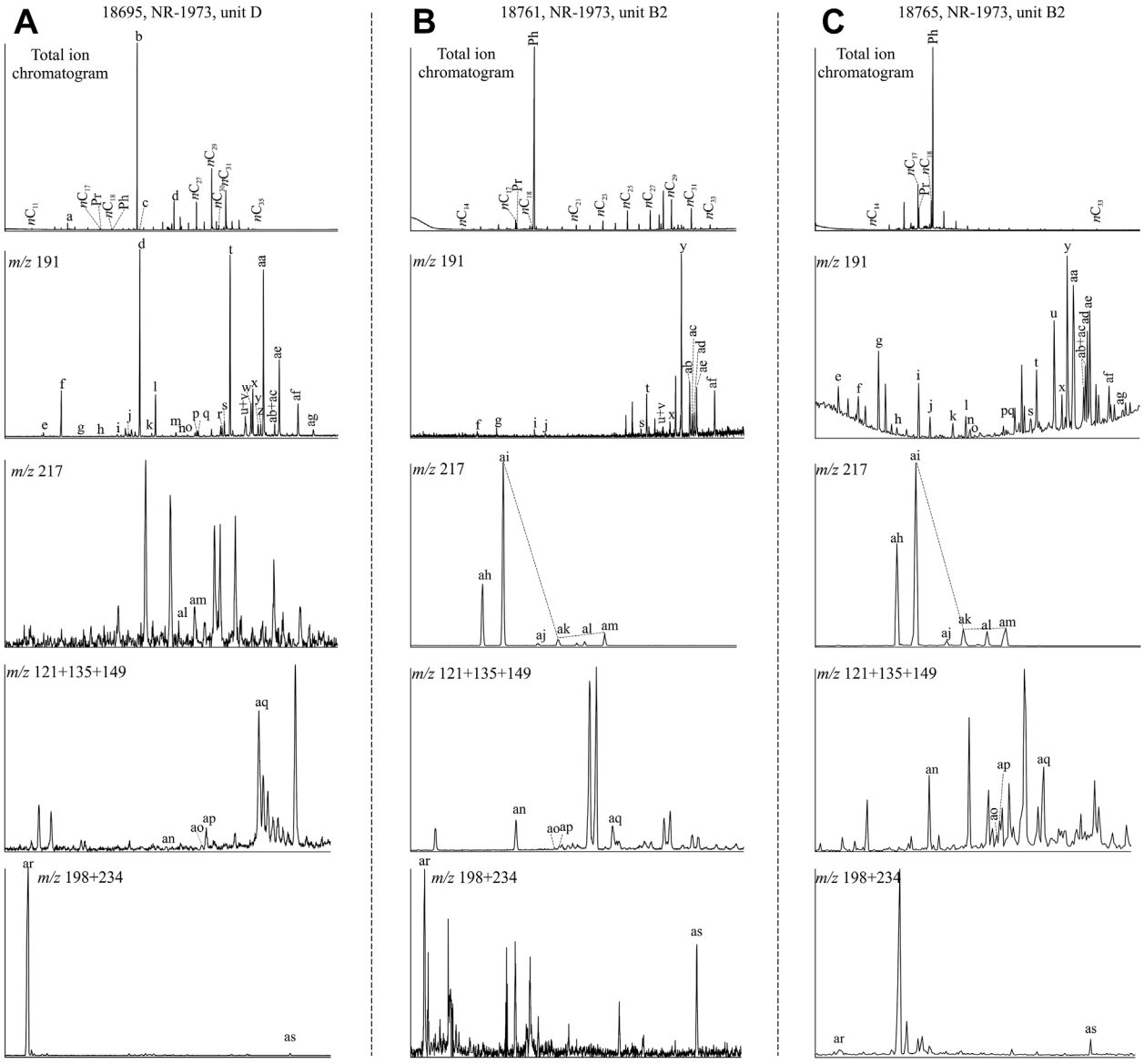


FIGURE 4
Total ion chromatograms and mass chromatograms of extractable lipids from the post-impact sediments in the Nördlinger Ries (assignments to the identified peaks see Table 1). Chromatograms for **(A)** coaly shale in uppermost unit D with a maximum of *n*-alkanes in the long chain range, **(B)** one of few samples with a weak bimodal *n*-alkane distribution (unit B2), and **(C)** a typical sample from unit B in the Nördlinger Ries (also unit B2) showing a maximum in the short chain *n*-alkane range. *m/z* 191 traces show hopanoids distribution; *m/z* 217 shows steranes distribution; *m/z* 121+135+149 traces shows the MTTCs distribution and *m/z* 198+234 traces present retene and cadalene. See Figure 2 for stratigraphic units.

ASE 150 device using dichloromethane (DCM) as the solvent. Drying and desulfurization of the raw extracts were performed with anhydrous $Na_2SO_4$ and activated copper powder. The extracts were subsequently fractionated by column chromatography over 2 g activated silica gel using 5 ml *n*-pentane for aliphatics, 5 ml of a mixture of *n*-pentane and DCM (v:v=4:6) for aromatics, 5 ml DCM for semi-polar compounds and 5 ml methanol for polar compounds successively as eluents (Schwarzbauer et al., 2000).

Derivatization of fatty acids in the polar fraction was completed according to the following procedures. The polar fraction was firstly dried and then diluted by about 0.5 ml methanol and subsequently reacted with the presence of 1 ml boron trifluoride diethyl etherate in a cap-screwed 8 ml vial at 70°C for 2 h. Subsequently, 2 ml deionized water was added to terminate the reaction, and 3 ml diethylether was then added to the mixture and shaken for 3 min. After 10 min ventilation, when the phase separation appears, the upper ester phase was carefully

TABLE 1 Abbreviations for the assigned biomarker compounds in Figure 4.

| Peak no. | Name | Peak no. | Name |
|---|---|---|---|
| A | $C_{15}$ dicyclesesquiterpene | aa | $C_{29}$ 17β(H),21β(H)-norhopane |
| B | 16α(H)-phyllocladane | ab | $C_{31}$ 17α(H),21β(H)-30-homohopane (22S) |
| C | ent-16α(H)-kaurane | ac | $C_{31}$ 17α(H),21β(H)-30-homohopane (22R) |
| D | des-A-lupane | ad | gammacerane |
| E | $C_{19}$ TT | ae | $C_{30}$ 17β(H),21β(H)-hopane |
| F | $C_{20}$ TT | af | $C_{31}$ 17β(H),21β(H)-30-homohopane |
| G | $C_{21}$ TT | ag | $C_{32}$ 17β(H),21β(H)-30,31-dihomohopane |
| H | $C_{22}$ TT | ah | $C_{27}$ 5β(H),14α(H),17α(H)-cholestane (20R) |
| I | $C_{23}$ TT | ai | $C_{27}$ 5α(H),14α(H),17α(H)-cholestane (20R) |
| J | $C_{24}$ TT | aj | $C_{28}$ 5β(H),14α(H),17α(H)-cholestane (20R) |
| K | $C_{25}$ TT (S+R) | ak | $C_{28}$ 5α(H),14α(H),17α(H)-cholestane (20R) |
| L | $C_{24}$ TeT | al | $C_{29}$ 5β(H),14α(H),17α(H)-cholestane (20R) |
| M | $C_{25}$ TeT | am | $C_{29}$ 5α(H),14α(H),17α(H)-cholestane (20R) |
| N | $C_{26}$ TT (R) | an | monomethyl 2-methyl-2-(4, 8, 12-trimethyl-tridecyl) chromans (δ-MTTC) |
| O | $C_{26}$ TT (S) | ao | dimethyl 2-methyl-2-(4, 8, 12-trimethyl-tridecyl) chromans (β-MTTC) |
| P | $C_{28}$ TT (R) | ap | dimethyl 2-methyl-2-(4, 8, 12-trimethyl-tridecyl) chromans (γ-MTTC) |
| Q | $C_{28}$ TT(S) | aq | trimethyl 2-methyl-2-(4, 8, 12-trimethyl-tridecyl) chromans (α-MTTC) |
| R | $C_{29}$ neohop-13 (18)-ene | ar | cadalene |
| S | 18α(H)-22,29,30-trisnorneohopane (Tm) | as | retene |
| T | 18β(H)-22,29,30-trisnorneohopane (βTm) | | |
| U | $C_{29}$ 17α(H),21β(H)-norhopane | | |
| V | $C_{29}$ Ts | | |
| W | $C_{30}$ hop-17 (21)-ene | | |
| X | $C_{29}$ 17β(H),21α(H)-norhopane | | |
| Y | $C_{30}$ 17α(H),21β(H)-hopane | | |
| Z | $C_{30}$ neohop-13 (18)-ene | | |

*TT, 13β(H),14α(H) tricyclicterpane, TeT=tetracyclicterpane, $C_{29}$ Ts= 18a,21b(H)-30-norneohopane.

transferred to a pointed flask using a pipette. Then 3 ml diethylether were added to the remaining sample, followed by shaking, ventilation and transformation actions for completely extracting derivative products, and all the reaction products (ester phase) were finally transferred with a pipette to the pointed flask. After evaporation to around 1 ml, the product was dehydrated with anhydrous $Na_2SO_4$ and solvent changed to DCM for further fractionation. The derivatization product was subsequently fractionated by column chromatography over 1 g activated silica gel into two fractions. The first fraction was eluted with 3 ml mixture of pentane and DCM (v:v=4:6) and then 6 ml DCM successively, and the second fraction was eluted with 5 ml methanol. The target derivatized polar compounds (i.e., fatty acids in form of esters) are in the first fraction.

Aliphatic, aromatic, semi-polar and derivatized polar fractions were measured by gas chromatography-flame ionization detector (GC-FID) and GC-mass spectrometry (GC-MS). GC analysis was performed on a Fisons Instruments GC 8000 equipped with a ZB-1 fused silica column (Zebron, 30 m length, 0.25 mm inner diameter, 0.25 μm film thickness) and an FID. The initial oven temperature was set to 60°C (isothermally held 3 min), then increased to 310°C at 5°C/min and finally kept constant for 20 min. GC-MS measurements were carried out on a Carlo Erba Mega Series HRGC 5160 equipped with a ZB-5 fused silica column (Zebron, 30 m length, 0.25 mm internal diameter, 0.25 μm film thickness) linked to a quadrupole mass spectrometer (Trace MS, Thermoquest). The mass spectrometer was operated in electron impact ionization (EI) mode at 70 eV ionization energy and in low resolution full scan mode. Helium was used as carrier gas. The oven temperature was programed from 80°C (isothermally held for 3 min) and subsequently increased to 320°C at a rate of 3°C/min, and finally kept constant for 20 min at 320°C. Peak identification was based on mass spectra and retention times by comparison with mass spectral libraries and literature data. Compound ratios were calculated based on peak areas integrated from respective ion chromatograms.

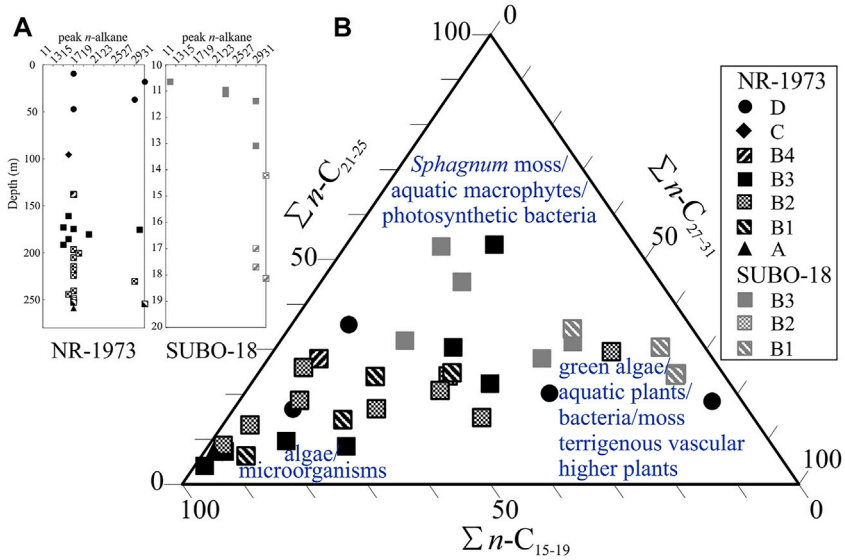


FIGURE 5
**(A)** Most prominent *n*-alkane peak versus depth and **(B)** chain length distribution of *n*-alkanes from the post-impact sediments in the Nördlinger Ries (Interpretation is based on Eglinton and Hamilton, 1967; Cranwell, 1977; dos Santos Neto et al., 1998; Ficken et al., 2000). Calculation is based on the integrated area in gas chromatograms. See Figure 2 for stratigraphic units.

## 3.5 Compound-specific stable carbon isotope analyses

Prior to analyses, selected aliphatic fractions were solvent changed to *iso*-octane and *n*-alkanes were subsequently removed using a zeolite molecular sieve ($SiO_2$:$Al_2O_3$=50:1). GC-FID was performed on the filtered fraction to check whether all *n*-alkanes were removed. Stable carbon isotope measurements were performed on a Finnigan Delta Plus XL mass spectrometer connected to a Fisons Instruments GC 6980A (equipped with a Zebron ZB-5 fused silica column of 60 m length, 0.25 mm internal diameter and 0.25 µm film thickness) via a GCC III combustion interface (gas chromatography-isotope ratio monitoring-mass spectrometry, GC-irmMS). One microliter of the sample was injected in splitless-mode at an injector temperature of 270°C. The oven temperature was programmed to 60°C (isothermally held for 3 min) and subsequently increased to 310°C at a rate of 3°C/min. Helium was used as carrier gas with a velocity of 35 cm/s. The eluting compounds were oxidized by a CuO/NiO/Pt-catalyst at 940°C. The carbon isotope ratio ($\delta^{13}C$) for the reference gas was calibrated with a reference standard from Chiron (Trondheim, Norway). Each sample was measured in triplicate, and averaged data of the three runs are expressed in the δ-notation relative to the VPDB standard. Further experimental details are given by Schwarzbauer et al. (2013).

## 3.6 Organic petrology

To investigate maceral composition and vitrinite reflectance (VRr), 14 whole-rock core samples (8 from NR-1973, six from SUBO-18) cut perpendicularly to bedding were microscopically analyzed adopting the procedures described in Littke et al. (2012). VRr measurements were carried out on a Zeiss Axioplan microscope (×500 magnification) in oil immersion at a wave length of 546 nm using a Leuco-Saphire standard (0.592% reflectance) for calibration prior to each measurement. Data were acquired and processed with the Diskus-Fossil software (Hilgers). Qualitative maceral identification and microphotographic documentation were conducted on a Zeiss Axio Imager.M2 in both incident white light and fluorescence mode.

# 4 Results

## 4.1 Elemental analysis

TOC contents in borehole NR-1973 mainly range from 2 wt % to 10 wt% with an average of 7.65 wt%, and only six samples show values lower than 2 wt%. Apparently three peaks occur in units B1, B3 and D, where TOC values reach up to 17 wt%, 25 wt %, and 27 wt%, respectively (Supplementary Appendix Table A1;

TABLE 2 Molecular geochemical parameters related to aliphatic and aromatic hydrocarbons of the post-impact sediments in the NR (CPI= carbon preference index, TAR= terrigenous/aquatic ratio, Paq=(n-C23+n-C25)/(n-C23+n-C25+n-C29+n-C31), Pr=pristane, Ph=phytane, n.d.=not determined;

| Sample | Unit | Depth (m) | *n*-$C_{15-19}$ (%) | *n*-$C_{21-25}$ (%) | *n*-$C_{27-31}$ (%) | CPI | TAR | Paq | Pr/ *n*-$C_{17}$ | Ph/ *n*-$C_{18}$ | Pr/ Ph | des-A-lupane/ DTPs | DTPs/ $C_{30}$ αβ hopane | Gamma cerane index | $C_{35}$- /$C_{31-35}$- homohop-17(21)-enes | $C_{27}$ sterane (%) | $C_{28}$ sterane (%) | $C_{29}$ sterane (%) | $C_{27-29}$ regular steranes/ $C_{29-32}$ 17α21β hopanes | DTPs/ $C_{27}$ sterane | retene/( retene+c adalene) | α/ total MMTC | δ/ total MMTC |
|---|---|---|---|---|---|---|---|---|---|---|---|---|---|---|---|---|---|---|---|---|---|---|---|
| 18/692 | D | 9.60 | 74 | 17 | 10 | 3.16 | 0.19 | 0.54 | 0.37 | 0.80 | 0.61 | 0.78 | 31.08 | 0.19 | n.d. | 35 | 14 | 51 | 0.38 | 72.87 | 0.23 | 0.68 | 0.03 |
| 18/693 | D | 18.25 | 30 | 20 | 50 | 4.41 | 2.41 | 0.31 | 0.30 | 1.15 | 0.37 | 0.44 | 1.10 | 0.19 | n.d. | 27 | 16 | 57 | 1.43 | 1.06 | 0.06 | 0.81 | 0.01 |
| 18/695 | D | 37.15 | 5 | 18 | 77 | 5.46 | 23.22 | 0.17 | 0.52 | 0.33 | 2.19 | 0.12 | 197.45 | 0.03 | n.d. | n.d. | n.d. | 100 | 0.05 | n.d. | 0.00 | 0.86 | 0.01 |
| 18/696 | D | 47.20 | 55 | 36 | 9 | 3.90 | 0.29 | 0.84 | 0.05 | 0.58 | 0.16 | 0.25 | 16.41 | 0.09 | n.d. | 29 | 61 | 11 | 0.05 | 255.35 | 0.18 | 0.90 | 0.00 |
| 18/697 | C | 95.53 | 90 | 7 | 3 | 1.79 | 0.04 | 0.78 | 0.30 | 0.71 | 0.99 | 0.66 | 1.36 | 0.18 | n.d. | 39 | 18 | 43 | 0.46 | 3.34 | 0.73 | 0.99 | 0.00 |
| 18/698 | B4 | 137.70 | 64 | 28 | 8 | 6.61 | 0.17 | 0.77 | 0.38 | 17.87 | 0.07 | n.d. | n.d. | 0.21 | n.d. | 68 | 25 | 7 | 12.43 | n.d. | 0.19 | 0.65 | 0.12 |
| 18/701 | B3 | 160.80 | 89 | 7 | 3 | 4.10 | 0.06 | 0.69 | 0.38 | 3.79 | 0.20 | n.d. | 0.38 | 0.10 | n.d. | 76 | 7 | 17 | 16.12 | 0.02 | 0.35 | 0.55 | 0.43 |
| 18/704 | B3 | 172.70 | 69 | 8 | 22 | 0.61 | 0.13 | 0.37 | 0.08 | 24.25 | 0.02 | 0.09 | 0.26 | 0.08 | n.d. | 75 | 11 | 14 | 13.77 | 0.01 | 0.43 | 0.32 | 0.60 |
| 18/711 | B3 | 174.40 | 41 | 30 | 29 | 2.26 | 0.81 | 0.41 | 0.52 | 37.18 | 0.05 | 0.24 | 4.45 | 0.10 | n.d. | 75 | 10 | 15 | 20.39 | 0.14 | 0.44 | 0.24 | 0.68 |
| 18/714 | B3 | 175.30 | 39 | 22 | 39 | 0.30 | 0.26 | 0.50 | 0.10 | 27.41 | 0.01 | 0.15 | 0.85 | 0.04 | n.d. | 70 | 14 | 16 | 18.74 | 0.05 | 0.69 | 0.18 | 0.78 |
| 18/717 | B3 | 180.10 | 23 | 53 | 24 | 1.22 | 1.15 | 0.68 | 0.47 | 0.54 | 0.48 | n.d. | n.d. | 0.12 | n.d. | 53 | 25 | 22 | 1.03 | n.d. | 0.34 | 0.05 | 0.60 |
| 18/723 | B3 | 185.20 | 94 | 4 | 2 | 4.74 | 0.02 | 0.72 | 0.54 | 13.94 | 0.20 | 0.34 | 0.38 | 0.14 | n.d. | 75 | 7 | 18 | 10.85 | 0.03 | 0.98 | 0.27 | 0.71 |
| 18/728 | B3 | 191.20 | 78 | 10 | 12 | 1.83 | 0.13 | 0.40 | 0.32 | 19.30 | 0.04 | 0.06 | 1.55 | 0.08 | n.d. | 68 | 9 | 24 | 14.84 | 0.07 | 0.35 | 0.30 | 0.65 |
| 18/733 | B2 | 196.20 | 44 | 15 | 41 | 0.94 | 0.58 | 0.40 | 0.26 | 35.90 | 0.04 | n.d. | n.d. | 0.15 | n.d. | 76 | 7 | 17 | 22.69 | n.d. | 0.39 | 0.00 | 0.97 |
| 18/740 | B2 | 200.10 | 72 | 19 | 10 | 3.95 | 0.21 | 0.44 | 0.27 | 0.73 | 0.24 | n.d. | n.d. | 0.45 | 0.07 | 67 | 17 | 16 | 8.46 | n.d. | 0.21 | 0.52 | 0.27 |
| 18/742 | B2 | 204.80 | 82 | 13 | 4 | 7.86 | 0.07 | 0.63 | 0.39 | 155.04 | 0.02 | 0.25 | 0.11 | 0.04 | 0.03 | 69 | 12 | 19 | 22.58 | 0.01 | 0.18 | 0.19 | 0.79 |
| 18/748 | B2 | 214.20 | 45 | 24 | 31 | 5.22 | 0.98 | 0.44 | 0.43 | 28.68 | 0.05 | n.d. | n.d. | 0.14 | n.d. | 94 | 3 | 4 | 20.30 | n.d. | 0.77 | 0.24 | 0.67 |
| 18/750 | B2 | 217.80 | 48 | 21 | 31 | 6.15 | 0.79 | 0.39 | 0.50 | 173.05 | 0.03 | n.d. | n.d. | 0.13 | n.d. | 92 | 5 | 3 | 97.67 | n.d. | 0.91 | 0.32 | 0.60 |
| 18/756 | B2 | 223.90 | 67 | 26 | 7 | 8.59 | 0.15 | 0.77 | 0.52 | 47.91 | 0.02 | n.d. | n.d. | 0.13 | 0.22 | 92 | 3 | 5 | 104.97 | n.d. | 0.79 | 0.23 | 0.69 |
| 18/761 | B2 | 230.10 | 16 | 29 | 55 | 4.01 | 4.73 | 0.35 | 0.82 | 86.25 | 0.02 | n.d. | n.d. | 0.12 | n.d. | 89 | 5 | 6 | 16.40 | n.d. | 0.31 | 0.42 | 0.51 |
| 18/765 | B2 | 240.00 | 89 | 9 | 2 | 4.71 | 0.04 | 0.75 | 0.55 | 8.39 | 0.10 | n.d. | n.d. | 0.30 | n.d. | 80 | 8 | 12 | 14.14 | n.d. | 0.58 | 0.31 | 0.50 |
| 18/768 | B2 | 243.80 | 60 | 17 | 23 | 4.85 | 0.61 | 0.43 | 0.43 | 7.67 | 0.17 | 0.22 | 0.30 | 0.11 | 0.08 | 66 | 24 | 10 | 8.25 | 0.03 | 0.20 | 0.43 | 0.40 |
| 18/773 | B1 | 247.90 | 87 | 6 | 7 | 8.63 | 0.08 | 0.48 | 0.01 | 32.28 | 0.03 | 0.28 | 0.28 | 0.57 | 0.07 | 64 | 22 | 14 | 13.25 | 0.02 | 0.28 | 0.60 | 0.19 |
| 18/776 | B1 | 250.00 | 57 | 24 | 19 | 7.18 | 0.54 | 0.57 | 0.29 | 1.88 | 0.38 | 0.35 | 1.12 | 0.31 | 0.31 | 70 | 14 | 16 | 5.29 | 0.20 | 0.60 | 0.50 | 0.10 |
| 18/778 | B1 | 252.50 | 67 | 14 | 19 | 10.80 | 0.34 | 0.39 | 0.08 | 1.83 | 0.30 | 0.42 | 0.14 | 0.73 | 0.33 | 64 | 16 | 19 | 5.32 | 0.01 | 0.16 | 0.60 | 0.15 |
| 18/780 | B1 | 253.90 | 44 | 25 | 31 | 14.15 | 1.00 | 0.38 | 0.33 | 7.65 | 0.13 | n.d. | 0.14 | 0.81 | 0.07 | 35 | 32 | 33 | 0.45 | 0.09 | 0.50 | 0.76 | 0.03 |
| 18/785 | A | 258.30 | 91 | 7 | 1 | 5.79 | 0.02 | 0.74 | 0.26 | 0.88 | 0.73 | n.d. | n.d. | 0.65 | 0.10 | 62 | 20 | 18 | 0.29 | n.d. | 0.62 | 0.24 | 0.17 |
| 20/294 | B3 | 10.67 | 48 | 32 | 20 | 5.46 | 0.62 | 0.63 | 0.43 | 3.93 | 0.20 | 0.74 | 2.05 | 0.28 | 0.04 | 32 | 40 | 28 | 1.87 | 1.88 | 0.59 | 0.82 | 0.02 |
| 20/299 | B3 | 10.98 | 31 | 53 | 16 | 8.45 | 0.49 | 0.82 | 0.16 | 60.19 | 0.06 | 0.66 | 1.62 | 0.44 | 0.06 | 41 | 45 | 13 | 5.83 | 0.30 | 0.33 | 0.86 | 0.01 |
| 20/301 | B3 | 11.13 | 32 | 45 | 23 | 6.58 | 0.73 | 0.70 | 0.18 | 30.25 | 0.07 | n.d. | 2.98 | 0.51 | 0.03 | 50 | 38 | 12 | 2.93 | 0.67 | 0.12 | 0.81 | 0.01 |
| 20/304 | B3 | 11.40 | 21 | 32 | 48 | 10.64 | 2.90 | 0.41 | 0.22 | 16.69 | 0.06 | n.d. | 1.40 | 0.53 | 0.01 | 36 | 53 | 11 | 2.65 | 1.05 | 0.01 | 0.84 | 0.05 |
| 20/322 | B3 | 13.10 | 28 | 28 | 44 | 7.28 | 2.44 | 0.38 | 0.31 | 3.54 | 0.21 | 0.52 | 0.90 | 0.70 | 0.05 | 31 | 38 | 31 | 2.84 | 0.35 | 0.14 | 0.87 | 0.00 |
| 20/335 | B2 | 14.23 | 7 | 25 | 68 | 3.88 | 14.55 | 0.23 | 0.28 | 1.27 | 0.21 | 0.66 | 2.18 | 0.14 | 0.01 | 43 | 24 | 33 | 0.83 | 2.59 | 0.53 | 0.37 | 0.12 |
| 20/362 | B1 | 17.00 | 19 | 35 | 46 | 10.39 | 3.80 | 0.44 | 0.52 | 11.82 | 0.11 | n.d. | 1.01 | 0.88 | 0.01 | 30 | 44 | 26 | 1.51 | 0.97 | 0.01 | 0.84 | 0.02 |
| 20/370 | B1 | 17.70 | 7 | 31 | 62 | 6.68 | 11.30 | 0.39 | 0.32 | 19.71 | 0.04 | n.d. | 0.59 | 0.51 | 0.06 | 11 | 25 | 64 | 2.65 | 0.47 | 0.01 | 0.83 | 0.02 |
| 20/374 | B1 | 18.13 | 8 | 24 | 68 | 3.04 | 12.25 | 0.31 | 0.40 | 1.30 | 0.37 | 0.75 | 0.51 | 0.15 | 0.02 | 4 | 8 | 88 | 6.48 | 1.19 | 0.14 | 0.90 | 0.00 |



10.3389/feart.2022.989478

Figure 3). Borehole SUBO-18 shows generally lower TOC values (0.15–12.6 wt%, average at 1.94 wt%) than borehole NR-1973. Its Miocene sequence represents two TOC peaks in the bottom (18.13 m) and middle (10.98 m) part similar to NR-1973 (253.9 and 175.3 m, respectively). TIC contents represent carbonate minerals. Depending on the presence of either dolomite or calcite, carbonate contents are roughly 8 times higher than TIC contents. TIC ranges in borehole NR-1973 from 0 to 12.2 wt% (average at 1.90 wt%) and in borehole SUBO-18 (0.01–9.1 wt%, average at 1.94 wt%); the highest values are found at the bottom succession (255.2 and 18.8 m, respectively), with a second peak in the middle of the sedimentary column (186.5 and 11.2 m, respectively). Additionally, a peak TIC value occurs at around 15 m in the SUBO-18. TS values in both boreholes do not show a significant trend and mostly range from 1–5 wt% (0.09–11.83 wt%, average at 2.04 wt% for NR-1973; 0.18–9.33 wt%, average at 2.95 wt% for SUBO-18).

## 4.2 Rock-Eval pyrolysis

$S_1$ values represent free and sorbed hydrocarbons (0.08–23.61 mg HC/g rock, average 3.37 mg HC/g rock for NR-1973; 0.02–7.02 mg HC/g rock, average 0.54 mg HC/g rock for SUBO-18) and show two peaks in the middle and the bottom of the borehole, in the depth interval, where peak TOC values occur. Hydrogen index (HI=$S_2$/TOC, Espitalié et al., 1985) fluctuates between 12 and 967 mg HC/g TOC in the NR-1973 (average at 447 mg HC/g TOC) with two prominent peaks in the middle (172.7 m) and bottom (248.9 m) part. Overall, the SUBO-18 borehole exhibits lower HI values compared to the NR-1973, having two clear peak intervals at 10.98 and 17 m depth (mean value 206 mg HC/g TOC; Figure 3). $T_{max}$ in the NR-1973 shows low values in the top and bottom part of the sequence with most samples ranging between 420 and 435°C (mean value 425°C). The SUBO-18, however, presents rather complex $T_{max}$ results oscillating from 352 to 453°C with a mean value of 411°C without an apparent depth trend (Figure 3).

## 4.3 Molecular organic geochemistry

### 4.3.1 Normal alkanes and isoprenoids

Total ion as well as selected ion chromatograms for the aliphatic fraction, and their assignments are shown in Figure 4 and Table 1, respectively. Figures 4A,B represent some rather special samples, whereas Figure 4C represents the typical composition of most samples. For the NR-1973, *n*-alkanes generally peak at *n*-$C_{15}$/*n*-$C_{17}$ and occasionally at *n*-$C_{29}$/*n*-$C_{31}$ (Figure 5A), while *n*-alkanes in the SUBO-18 generally peak at *n*-$C_{23}$/*n*-$C_{29}$/*n*-$C_{31}$. Most samples display a unimodal distribution (Figures 4A,C), while a few samples have a weak bimodal distribution for the *n*-alkanes (Figure 4B). Chain length of *n*-alkanes for most samples varies from *n*-$C_{11}$ to *n*-$C_{35}$, depicting a predominance of short-to intermediate-chain *n*-alkanes (Figures 4C, 5B). Carbon preference index (CPI= [(*n*-$C_{25}$+*n*-$C_{27}$+*n*-$C_{29}$+*n*-$C_{31}$+*n*-$C_{33}$)/(*n*-$C_{24}$+*n*-$C_{26}$+*n*-$C_{28}$+*n*-$C_{30}$+*n*-$C_{32}$)+(*n*-$C_{25}$+*n*-$C_{27}$+*n*-$C_{29}$+*n*-$C_{31}$+*n*-$C_{33}$)/(*n*-$C_{26}$+*n*-$C_{28}$+*n*-$C_{30}$+*n*-$C_{32}$+*n*-$C_{34}$)]/2, Bray and Evans, 1961) values are generally much higher than 1 (Table 2), implying immature OM in the sediments. The ratio of *n*-$C_{27}$/*n*-$C_{17}$ is mostly very low (<1, Table 2) with the highest value in the coaly shale in unit D (sample 18/695) at the central site. Usually, this ratio is very well suitable in order to distinguish input of terrestrial organic matter versus marine, aquatic organic matter. However, in the case of the very special NR lake sediments, it does not work well, because concentrations of both *n*-$C_{27}$ and *n*-$C_{17}$ are very low. Furthermore, the ratio of (*n*-$C_{15}$+*n*-$C_{17}$)/(*n*-$C_{23}$+*n*-$C_{25}$) is mostly larger than 1, being in line with the predominant contribution of algae over macrophytes. Also, values of the terrigenous/aquatic ratio (TAR=(*n*-$C_{27}$+*n*-$C_{29}$+*n*-$C_{31}$)/(*n*-$C_{15}$+*n*-$C_{17}$+*n*-$C_{19}$), Bourbonniere and Meyers, 1996) are commonly lower than 1 (Table 2; Figure 6A), except in the coaly shale sample (18/695) in unit D (NR-1973) and the lower sequence in the SUBO-18 having high values. Paq (Paq=(*n*-$C_{23}$+*n*-$C_{25}$)/(*n*-$C_{23}$+*n*-$C_{25}$+*n*-$C_{29}$+*n*-$C_{31}$), Ficken et al., 2000) is usually above 0.4, except for the middle unit D (ca. 18–38 m) in borehole NR-1973 and the bottom succession (e.g., 13–15 m and below 17 m) of borehole SUBO-18 (Table 2; Figure 6A).

Amongst isoprenoids, Pr and Ph are the predominant compounds, and Ph is even the highest peak dominating over all other compounds in all the samples except in NR-1973 unit.

D and the bottom of borehole SUBO-18 (Figure 4). Values of Pr/*n*-$C_{17}$ range between 0.01 and 0.82 with most of the values being less than 0.6 (Table 2; Figure 7), while values of Ph/*n*-$C_{18}$ span from 0.33 to 173.0 (Table 2; Figure 7). Pr/Ph is observed to vary from 0.01 to 2.19 with most samples below 0.5; the only high value occurs in the coaly shale sample in unit D (Table 2; Figure 6A).

### 4.3.2 Diterpenes, tricyclic terpanes and hopanoids

Diterpenes (DTPs) were evaluated based on the *m/z* 123 mass trace. Tricyclic terpanes (ranging from $C_{19}$ to $C_{28}$, except $C_{27}$). Hopanes (ranging from $C_{27}$ to $C_{32}$) were identified based on the *m/z* 191 mass trace (Figure 4), and hopenes (range from $C_{30}$ to $C_{35}$) were identified on the *m/z* 367 mass trace. Diterpenoids are mainly composed of 4β(H)-19-norisopimarane, 16α(H)- phyllocladane, ent-16α(H)-kaurane and *des*-A-lupane in the studied samples, but not all the samples contain all the four diterpenoids. According to the *m/z* 191 mass trace, peaks of pentacyclic triterpenoids are generally much higher than those of tricyclic terpanes (Figure 4). Among $C_{27}$ trisnorhopenoids, 18α(H)-22,29,30-trisnorneohopane (Ts) is absent and 17α(H)-22,29,30-trisnorhopane (Tm) occurs in low concentration, while 17β(H)-22,29,30-trisnorhopane (βTm) is abundant in both boreholes, which is in line with immature OM. $C_{29}$ 17β(H),21β(H) norhopane ($C_{29}$ ββ hopane) gradually becomes predominant in *m/z* 191 with increasing depth in borehole NR-

1973. The dominant peak in *m/z* 191 for borehole SUBO-18 is either $C_{29}$ ββ hopane or $C_{30}$ hop-17 (21)-ene or $C_{29}$ 17β(H),21α(H) hopane without a clear trend. The typical biological 17β(H),21β(H) hopanes (range from $C_{29}$ to $C_{32}$) are dominant over their corresponding geological isomers (17α(H),21β(H)), suggesting that biomolecules remain at a low transformation stage. The 17 α(H),21β(H) isomers only reach $C_{31}$, while the homohop-17 (21)-enes reach $C_{35}$, but these extended molecules only occur in the lower sequence of borehole NR-1973 (i.e., units B2, B1 and A), and in borehole SUBO-18.

High total diterpenoids/$C_{30}$ αβ hopane (DTPs/$C_{30}$ αβ hopane) values suggest higher contributions of higher land plants (especially gymnosperms) to OM relative to prokaryotes. As shown in Figure 6B, DTPs/$C_{30}$ αβ hopane shows a roughly ascending trend (0–197.45) from bottom to top in borehole NR-1973 with some samples having no diterpenoids at all. In contrast, this ratio increases from 0.51 to 2.98 in borehole SUBO-18. Most $C_{29}$ αβ-/$C_{30}$ αβ hopane ratios are less than 1 (0.10–1.61, average at 0.51) in borehole NR-1973, while they tend to be higher (0.33–2.77; mean value 1.11) in borehole SUBO-18. Tetrahymanol as a precursor of gammacerane is principally sourced from bacterivorous ciliates, which feed on green/purple sulfur bacteria occurring under anaerobic conditions in stratified water columns. Thus gammacerane was proposed to reflect water column stratification (Sinninghe Damsté et al., 1995). Water column stratification in turn is related to water salinities and gammacerane is therefore also used to indicate bottom water salinities. Gammacerane/(gammacerane+$C_{30}$ αβ hopane) (gammacerane index) values are mainly below 0.2 (0.03–0.81, average 0.23) in borehole NR-1973 except for the bottom sequence (e.g., 250–260 m), while it varies mainly between 0.14 and 0.88 (average 0.46) in borehole SUBO-18. $C_{35}$-/$C_{31\text{-}35}$-homohop-17 (21)-enes ratios increase with decreasing bottom water oxygen content (Rullkötter and Philip, 1981) and are clearly higher in borehole NR-1973 (0.03–0.33, average 0.14) than in borehole SUBO-18 (0–0.06, average 0.03; Table 2).

### 4.3.3 Steranes

The regular steranes ($C_{27\text{-}29}$ steranes) were primarily recognized based on the *m/z* 217 ion chromatogram, while some unresolved methylsteranes with a molecular mass of 414 Da were found in *m/z* 231. The regular steranes are composed of six peaks, i.e., 5β,14α,17α (20R) and 5α,14α,17α(20R) configurations for $C_{27}$, $C_{28}$ and $C_{29}$ steranes, respectively (Figure 4). The explicit identification of 5β,14α,17α-sterane (20R) was not documented in the NR before, which is a biological configuration implying a very low thermal maturity in line with hopanoid species described above. The regular steranes represent an "L-shaped" distribution pattern indicating the absolute dominance of $C_{27}$ steranes in most samples (Figure 4). The normalized $C_{27}$ steranes to total regular steranes ratio ($C_{27}$ sterane (%)) of borehole NR-1973 (27–94%, average 66%) is clearly higher than that in borehole SUBO-18 (4–50%, average 31%) (Table 2; Figures 6C, 8). $C_{28}$ steranes (%) range between 3 and 61% (average 21%). It is a minor component in most samples from borehole NR-1973, but accounts for a relatively large percentage of steranes in borehole SUBO-18. The amount of $C_{29}$ steranes (%) ranges from 3 to 88% with a higher percentage in borehole SUBO-18 (average 34%) than in borehole NR-1973 (average 19%). It should be noted that almost no $C_{27}$ and $C_{28}$ regular steranes were found in the coaly shale sample (sample 18/695). The ratio of $C_{27\text{-}29}$ steranes/$C_{29\text{-}32}$ αβ hopanes ranges from 0.05 to 104.97 with higher values in the middle-lower sequence of borehole NR-1973, intermediate values in borehole SUBO-18 and low values in the upper part of the NR-1973 (Table 2; Figure 6C). Total diterpenoids/$C_{27}$ steranes (DTPs/$C_{27}$ sterane) ratio reflects the contribution from higher land plants to OM relative to algae. DTPs/$C_{27}$ sterane values range from 0.01 to 255.35 in borehole NR-1973, where high values only occur in unit D, while most of the samples have extremely low values; i.e., there is an absence of diterpenoids in part of the samples from units A and B. DTPs/$C_{27}$ steranes ratios for borehole SUBO-18 range from 0.30 to 2.59 and are generally slightly higher than in borehole NR-1973 (Table 2).

### 4.3.4 Polycyclic aromatics and heteroatomic compounds

Retene and cadalene were evaluated based on *m/z* 234 and 198 ion chromatograms, respectively. Mono-, di- and trimethyl 2-methyl-2-(4, 8, 12-trimethyltridecyl) chromans (δ-, β- and γ-, and α-MTTCs) were identified on *m/z* 121, 135 and 149, respectively. As presented in Figure 6B and Table 2, ratios of retene/(retene+cadalene) fluctuate between <0.01 and 0.98. Empirical observations suggested that the relative concentration α-MTTC (α-/total MTTC) decreases with increasing depositional water salinities, while there is an inverse trend for δ-MTTC; accordingly, α-/total MTTC in combination with Pr/Ph ratios is proposed to be indicative of water salinities, where Pr/Ph<0.2 and α-/total MTTC<0.5 suggest hypersaline conditions, Pr/Ph>0.2 and α-/total MTTC>0.5 indicate mesosaline conditions (as proven by Permian Kupferschiefer sediments, salt concentration 40–120‰), Pr/Ph>0.3 and α-/total MTTC>0.6 reflect marine-like water salinities (as proved by Upper Jurassic Malm, salt concentration 30–40‰) and Pr/Ph>1 and α-/total MTTC>0.7 reflect fresh water conditions (salt concentration 1–30‰) (Schwark et al., 1998; Wang et al., 2011; Jiang et al., 2019). The values of α-MTTC normalized to total MTTC compounds (α-/total MTTCs) vary from <0.01 to 0.99 with a mean value of 0.45 in borehole NR-1973, clearly lower than that in borehole SUBO-18 (0.37–0.90, average 0.79). The normalized δ-MTTC (δ-/total MTTC) ratios for borehole NR-1973 (0.001–0.97, average 0.39) are significantly higher than those in borehole SUBO-18 (0.004–0.12, average 0.03).

Both straight-chained esters in the semi-polar fraction and fatty acid esters (after derivatization) in the polar fraction were measured for samples from borehole NR-1973 and identified based on *m/z* 74 as representative. Samples from the marginal drilling were not included. Generally, straight-chain esters and *n*-alkanoic acids are the dominant compounds in semi-polar and

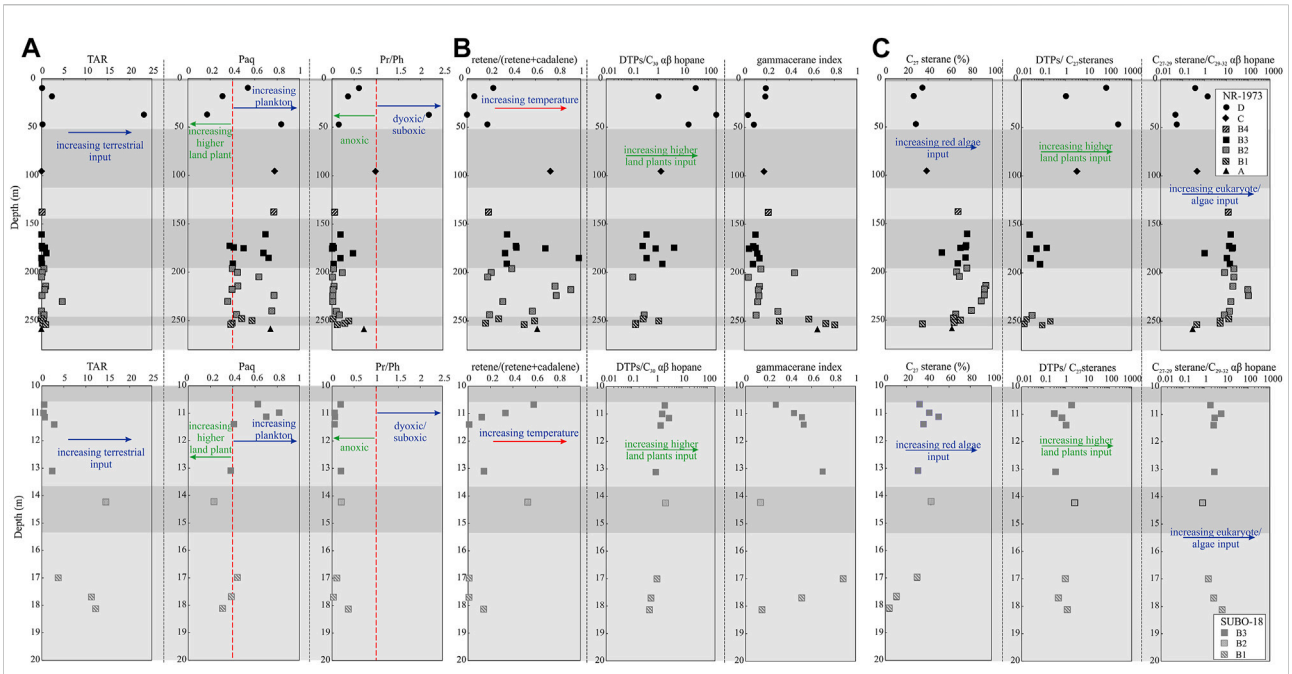


FIGURE 6
Molecular geochemical profiles of **(A)** *n*-alkanes and isoprenoids related proxies, **(B)** terpenoids and polycyclic aromatic hydrocarbons related proxies and **(C)** steranes related proxies for the post-impact sediments in the Nördlinger Ries. TAR = ($n$-$C_{27}$+$n$-$C_{29}$+$n$-$C_{31}$)/($n$-$C_{15}$+$n$-$C_{17}$+$n$-$C_{19}$), Paq = ($n$-$C_{23}$+$n$-$C_{25}$)/($n$-$C_{23}$+$n$-$C_{25}$+$n$-$C_{29}$+$n$-$C_{31}$), Pr = pristane, Ph = phytane, DTPs = diterpenes, gammacerane index = gammacerane/(gammacerane+$C_{30}$ αβ hopane). See Figure 2 for stratigraphic units.

polar fractions, respectively. Straight-chain esters range from $C_{15}$ to $C_{35}$ and mostly peak at $C_{17}$ in the examined samples. Exceptions appear in the coaly shale from unit D peaking at $C_{27}$, while samples from the bottom of the central well, i.e., samples 18/776 and 18/785, peak at $C_{25}$ and $C_{23}$, respectively. The normalized percentages of $C_{17–21}$ (short straight-chain esters, SSCE), $C_{23–27}$ (intermediate straight-chain esters, ISCE) and $C_{29–33}$ (long straight chain-esters, LSCE) are shown in Table 3. The proportion of SSCE accounts for 2–100% (60% on average) with an apparently low value in the coaly shale sample from unit D, and ISCE and LSCE account for 0–58% (30% on average) and 0–44% (9% on average), respectively. *N*-alkanoic acids as expressed in methyl esters peak at $C_{18}$/$C_{16}$ and range between $C_8$ to $C_{30}$, with low amounts of *iso*- and *anteiso*-structures. Normalized $C_{17–21}$ (short-chain *n*-alkanoic acid esters, SSCFE), $C_{23–27}$ (intermediate-chain *n*-alkanoic acid esters, ISCFE) and $C_{29–33}$ ratios (long-chain *n*-alkanoic acid esters, LSCFE) to their sum were calculated (Table 3). SSCFE dominantly span the range of 46–97% (85% on average), while ISCFE and LSCFE only account for 2–47% (13% on average) and 0–7% (1% on average), respectively.

## 4.4 Compound-specific stable carbon isotope analyses

$\delta^{13}C$ values of Pr vary between -33.8‰ and -26.1‰ for selected samples, while Ph is more enriched in $^{13}C$ resulting in $\delta^{13}C$ values of −28.2 to −25.1‰ (Table 3). The $\delta^{13}C$ value of Pr failed to be obtained when its concentration was extremely low compared to Ph. $\delta^{13}C$ values for $C_{27}$ steranes were evaluated for three samples, showing ranges of −28.2 to −23.6‰ and −29.0 to −24.2‰ for 5β,14α,17α(20R) and 5α,14α,17α(20R) configurations, respectively.

## 4.5 Organic petrology

In the samples derived from borehole NR-1973, macerals are mostly present in a fine-grained, laminated mineral matrix. Vitrinite and inertinite particles are most abundant and largest in the uppermost unit D, where inertinite is the dominant maceral group in samples 18/691 and 18/693 (Figure 9A), while vitrinite is predominant in sample 18/695 (Figure 9B). Because of the abundance of vitrinite, random vitrinite reflectance (VRr) was measured for samples in unit D, showing a value of 0.33%. The other samples analyzed contained either no or insufficient vitrinite for the measurement of VRr. Considering the low borehole temperature (<30°C) and the geological temperature history (Rullkötter et al., 1990), OM maturity for the deeper sediments is expected to be quite similar to that of unit D, i.e., OM in the NR is thermally immature. Down the section of borehole NR-1973, vitrinite and inertinite are either absent or extremely rare and small

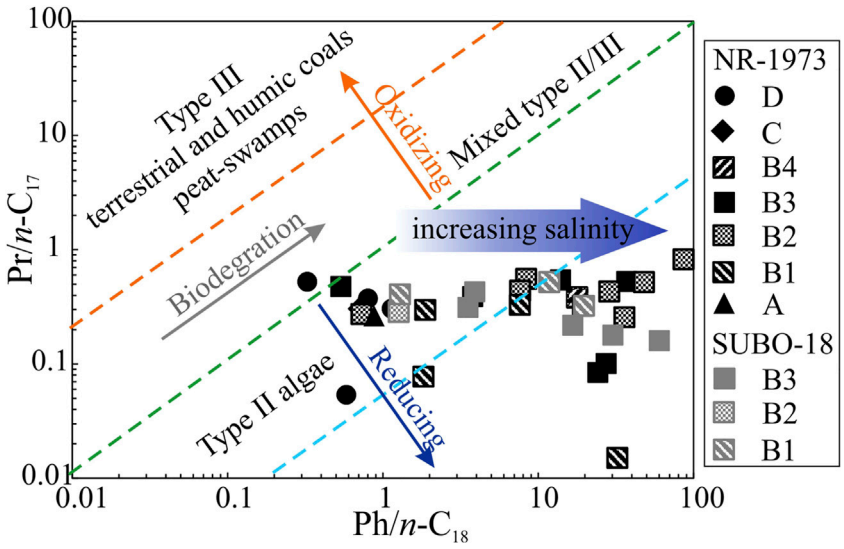


FIGURE 7
Crossplot of Pr/*n*-$C_{17}$ vs Ph/*n*-$C_{18}$ of the post-impact sediments in the Nördlinger Ries (modified after Shanmugam, 1985). See Figure 2 for stratigraphic units.

(Figures 9C,D) in samples taken from the deeper units C and B. Here, alginite having bright fluorescence is most abundant, occurring mostly as lamalginite (Figures 9E,F) and occasionally as telalginite, showing well-preserved structure (Figures 9G,H). Most samples show large amounts of amorphous organic matter with bright fluorescence. This unstructured fluorescent groundmass (UFG; Figures 9D,F,H,L) is especially dominant in samples taken from unit B. The strong background fluorescence indicates the presence of submicroscopically small (<1 μm), hydrogen-rich organic matter disseminated in between the mineral matrix.

In the six samples from borehole SUBO-18, vitrinite and inertinite particles are rare and small if observed, except for the lowermost sample (sample 20/374) having larger vitrinite/inertinite particles and a VRr of 0.32%. Alginite is the main species of liptinite observed here, showing bright yellow fluorescence (Figures 9K,L). UFG is abundant as well. Pyrite grains are mostly small, usually occurring as small framboids or single euhedral crystals.

# 5 Discussion

## 5.1 Chemostratigraphy

Chemostratigraphy is related to the description and correlation of strata on the basis of their chemical composition (Saraswati, 2015). Here, the distribution of TOC, $S_1$ and HI, combined with lithological differences in the two studied boreholes are adopted to develop a potential stratigraphic correlation scheme (Figure 2). Basically, all the recovered core sections from the central area (NR-1973) were deposited during the Miocene (Füchtbauer and von der Brelie, 1977), while deposits above 4.55 m in borehole SUBO-18 were reported to be Quaternary fluvial sediments (Arp et al., 2014). Consequently, Miocene sediments below 4.55 m in the stratigraphic column of borehole SUBO-18 are compared with the Miocene sequence of borehole NR-1973 in this study (Figure 2). In the TOC, $S_1$ and HI profiles for the SUBO-18 borehole, two prominent peaks are visible (Figure 3). These peaks are also visible in the central borehole, where much larger Miocene thicknesses are observed. Therefore, the two peaks in borehole SUBO-18 are attributed to marker signals corresponding to the two peak values in units B1 and B3 of borehole NR-1973, and are tentatively correlated with units B1 and B3 for the lower and upper marker layer, respectively (Figure 3).

As depicted in Figure 2, the lithology between 23 and 18.32 m is marlstone interbedded with calcareous sandstone in SUBO-18, and in conjunction with the rather low TOC, $S_1$ and HI values in this interval, this depth range is therefore designated as "basal marlstone (SBM)". Upwards, between 18.32 and 15.35 m, the lithology starts with oil shale (bitumen-rich claystone) and is followed mainly by marlstone with parallel bedding having the first peak in TOC, $S_1$ and HI values, and thus is correlated with unit B1. The oil shale in borehole SUBO-18 might be consistent with the oil shale at the bottom of borehole NR-1973 (Figure 2). Nevertheless, sediments between 23 and 15.35 m in borehole SUBO-18 are speculated to be syn-deposited with unit B1 in borehole NR-1973, because the suevite deposits downward from 25 m in borehole SUBO-18 should correlate with unit A (suevite in NR-1973) (Figure 2).

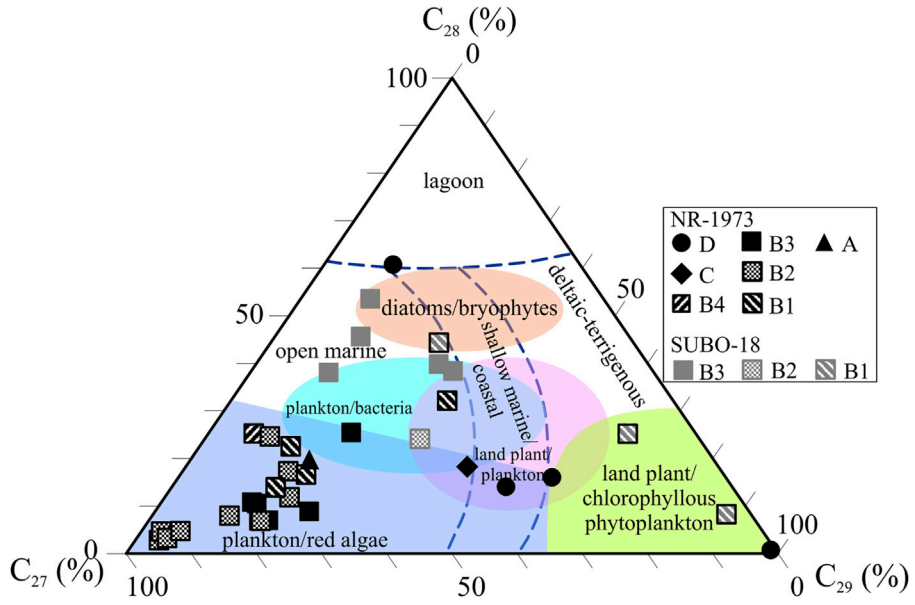


FIGURE 8
Triangle plot of regular $C_{27}$-, $C_{28}$- and $C_{29}$-steranes (%) normalized to the sum of all regular steranes for the post-impact sediments in the Nördlinger Ries (Modified after Huang and Meinschein, 1979; Volkman, 1986; Kodner et al., 2008). See Figure 2 for stratigraphic units.

Further upward, between 15.35 and 13.63 m in borehole SUBO-18, the lithology consists of marls and calcareous sandstone, and TOC, $S_1$ and HI values are rather low, coinciding with lower values in unit B2 of borehole NR-1973 compared to B1 and B3; thus, this interval is correlated with unit B2. The second peak in TOC, $S_1$ and HI values occurs in the interval of 13.63–10.65 m in borehole SUBO-18, which is composed of marlstone with either parallel bedding or slump structure. This depth interval correlates with unit B3 of borehole NR-1973, where also high TOC, $S_1$ and HI values are found. Between 10.65 and 4.55 m, the lithology shifts to laminated clay-marlstone, having rather low TOC, $S_1$ and HI values, which can be correlated to unit B4 in borehole NR-1973 (Figures 2, 3). It should be noted that different correlations were suggested by Arp et al. (2014, 2021); according to the latter one, Miocene units in the SUBO-18 well would correlate to units B1 and B2 in the center.

## 5.2 Kerogen type

In borehole NR-1973, OM in units A–C is mainly composed of type II kerogen based on Rock-Eval data, with type I kerogen present at the boundaries of unit B2, and in the middle of units B1 and B3 (Figure 10). Kerogen type in unit D shifts from type II to type III; i.e., there is an overall decreasing HI from bottom to the top of the profile (Figure 3). It should be noted that the H/C values (significantly over 1.5) of kerogens reveal typical type I kerogen in some post-impact sediments (Rullkötter et al., 1990), which slightly contradicts the interpretation of Rock-Eval results in this study. Large amounts of illite and smectite were documented to occur within the central sequence (Salger, 1977), which could impose an intense hydrocarbon retention effect on the mineral matrix thus reducing the $S_2$ and HI values (Yang and Horsfield, 2020). The same effect can be expected for zeolites. Therefore, the Rock-Eval $S_2$ and HI data might be biased by the retention of generated hydrocarbons on clay minerals or zeolites, and type I kerogens are still expected in units B1 and B3.

In borehole SUBO-18, OM is primarily composed of type II and III kerogen with clearly lower HI values, which vary less compared to those of borehole NR-1973. On the one hand, such differences seem to be reasonable, because the marginal domain in a basin can receive more terrigenous OM having lower hydrocarbon generation potential and thus lower HI values. On the other hand, the calculated HI values are expected to be lower than their authentic HI due to abundant illite and smectite in the marginal sequence (Arp et al., 2014), leading to hydrocarbon retention upon pyrolysis and thus lowered $S_2$ and HI values.

## 5.3 Depositional environment

### 5.3.1 Climate and water temperature

The higher plant parameter (HPP), which is defined as the relative concentration of retene and cadalene (HPP = retene/(retene + cadalene)), can be used to obtain insight into the paleo-

TABLE 3 Percentage of straight chain ester and alkanoic acid parameters (calculated to the sum of all esters or alkanoic acids, respectively) and compound-specific carbon isotope data of some specific biomarkers from post-impact sediments in borehole NR-1973 from the Nördniger Ries. n.d.=not determined.

| Sample | Unit | Depth (m) | Straight chain esters (%) | | | Straight chain fatty acid easters(%) | | | $\delta^{13}C$ (pristane, %) | $\delta^{13}C$ (phytane, %) | $\delta^{13}C$ ($C_{27}$ βααR sterane, %) | $\delta^{13}C$ ($C_{27}$ αααR sterane, %) |
|---|---|---|---|---|---|---|---|---|---|---|---|---|
| | | | $C_{17-21}$ | $C_{23-27}$ | $C_{29-33}$ | $C_{17-21}$ | $C_{23-27}$ | $C_{29-33}$ | | | | |
| 18/692 | D | 9.60 | 59 | 34 | 8 | 93 | 6 | 0 | -31.0 | -27.8 | | |
| 18/693 | D | 18.25 | 100 | 0 | 0 | 97 | 2 | 0 | | | | |
| 18/695 | D | 37.15 | 2 | 54 | 44 | | | | | | | |
| 18/697 | C | 95.53 | 80 | 17 | 3 | 92 | 7 | 1 | | | | |
| 18/698 | B4 | 137.70 | 48 | 42 | 10 | 93 | 7 | 0 | n.d. | n.d. | -28.2 | -29.0 |
| 18/701 | B3 | 160.80 | 40 | 52 | 8 | 84 | 16 | 0 | -30.3 | -25.1 | | |
| 18/717 | B3 | 180.10 | 100 | 0 | 0 | 78 | 20 | 2 | | | | |
| 18/723 | B3 | 185.20 | 40 | 50 | 11 | 98 | 2 | 0 | -27.7 | -27.1 | | |
| 18/733 | B2 | 196.20 | | | | | | | n.d. | -26.4 | | |
| 18/740 | B2 | 200.10 | 95 | 5 | 0 | 52 | 44 | 4 | -28.4 | -28.2 | | |
| 18/756 | B2 | 223.90 | 53 | 40 | 7 | 94 | 6 | 0 | -26.1 | -25.8 | -23.6 | -24.2 |
| 18/761 | B2 | 230.10 | 100 | 0 | 0 | 46 | 47 | 7 | n.d. | -26.9 | -24.9 | -26.5 |
| 18/776 | B1 | 250.00 | 24 | 58 | 18 | 82 | 17 | 0 | -33.8 | -27.2 | | |
| 18/778 | B1 | 252.50 | 95 | 5 | 0 | 66 | 33 | 1 | -32.7 | -26.1 | | |
| 18/785 | A | 258.30 | 38 | 58 | 4 | 92 | 8 | 0 | -31.8 | -26.6 | | |

botanical community (van Aarssen et al., 2000). High HPP (towards 1) suggests the presence of a large proportion of drought-tolerant plants, in particular conifers that produce retene (van Aarssen et al., 2000; Jiang et al., 2020). In borehole NR-1973, the ratio of retene/(retene+cadalene) varies widely in units B and C, while values are low in unit D (Figure 6B). The latter values can be explained by a very low amount of conifers in the direct vicinity of the lake; this fits the high paleotemperatures known for the Miocene in this area. The partly much higher values in units B and C (with much scatter) may be due to other sources of retene such as algae and bacteria (Wen et al., 2000), since higher land plants are extremely rare in this section.

In this study, glycerol dialkyl glycerol tetraether (GDGT) analysis was successfully conducted on one sample from unit D. Data reveal an annual mean paleo-water surface temperature of about 25°C at the very top of borehole NR-1973. This temperature is well in line with published GDGT-derived temperatures for Miocene lignite (~14.8 Ma) from western Germany (Stock et al., 2016).

## 5.3.2 Water salinity and stratification

MTTC related proxies have been widely used for reconstructing paleo-salinity of water bodies, and the crossplot of Pr/Ph vs α-/total MTTC turned out to be a powerful tool to reconstruct water salinity (e.g., Schwark et al., 1998; Wang et al., 2011; Jiang et al., 2019). The lake water in the crater center (NR-1973) was initially mesosaline (units A and B1, Figure 11). Later, water salinity increased to hypersaline in unit B2. After a short drawback to mesosaline conditions at late B2, water salinity raised back to hypersaline in unit B3, then continuously decreased to mesosaline in unit B4 and then to normal marine-like salinity in unit C. Unit D started from mesosaline and kept a normal-marine salinity except for a short term at fresh water conditions during which the coaly shale seam formed. Within the marginal area (SUBO-18), units B1, B2 and B3 experienced lower water salinities but the same evolutional trend as B1, B2 and B3 in the center, respectively, which is in agreement with the aforementioned stratigraphic correlation results. Such diversity in salinity might occur as heavier saline water tends to sink filling the deep part of the basin and thus leading to higher salinity proxies in central sediments.

High concentrations of gammacerane usually imply intense water column stratification (Sinninghe Damsté et al., 1995). Generally, the gammacerane index shows a decreasing trend from the basal part to unit B2 and subsequent maintenance of weak stratification in the central crater till the end, while the marginal lake shows stronger stratification levels (Figure 6B). The latter conclusion concerning a more intense water stratification in the shallow, marginal lake is not logical from a hydrological

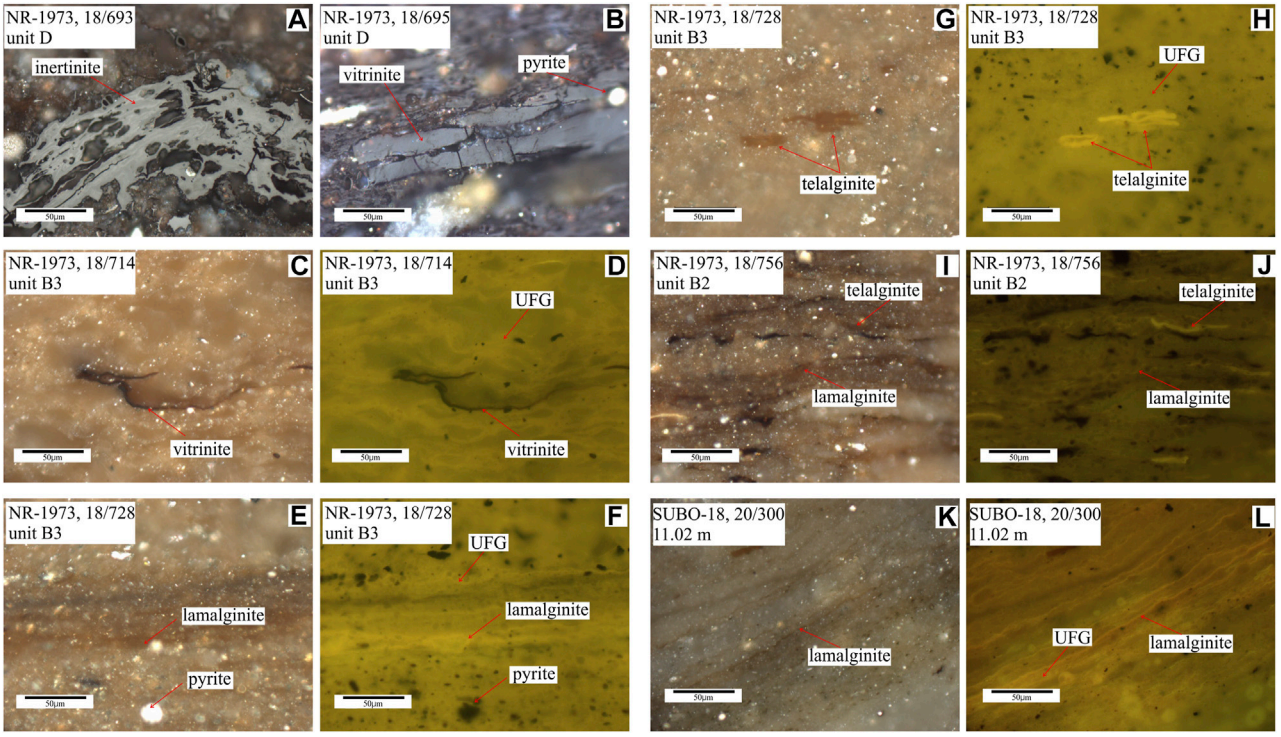


FIGURE 9
Maceral microphotographs of selected polished sections from the NR-1973 and SUBO-18. See Figure 2 for stratigraphic units. **(A,B,C,E,G,I,K)** are taken under white incident light; **(D,F,H,J,L)** show the fluorescence mode excited by UV-light.

point of view. In this context it should be mentioned that gammacerane is reported to be a diagenetic product of tetrahymanol (ten Haven et al., 1989), which appears to mainly originate from bacterivorous ciliates, occurring around the chemocline of stratified water columns feeding on bacteria (Sinninghe Damsté et al., 1995). Therefore, the differences in gammacerane index evolution between the analyzed two boreholes might be confined by the availability of prokaryotes, which will be discussed in more detail in the following section. The depletion of prokaryotes, over most of the time in the crater center, limits the development of bacterivorous ciliates (Figure 12A), leading to rather low and decreasing gammacerane production and a negative trend between gammacerane index and $C_{27\text{-}29}$ steranes/$C_{29\text{-}33}$ αβ hopanes (Figure 12B).

High concentrations of δ-MTTC or low concentrations of α-MTTC suggest high water salinity (Schwark et al., 1998; Jiang et al., 2018). A positive correlation was found between δ-/total MTTC and the gammacerane index in some previous cases, revealing that a higher water salinity enhances the stratification of the water column (Jiang et al., 2018). Nonetheless, the gammacerane index partly shows a negative correlation with the δ-/total MTTCs in this study (Figure 12C), which was observed in other studies as well, e.g., Zhang et al. (2012) and Tulipani et al. (2015). Such negative correlation might be explained by intense water stratification, which does not favor the mix of the hypersaline bottom water and the less-saline upper water body based on studies of the lacustrine Messinian (Kenig et al., 1995) and Oligocene successions from the Qaidam Basin (Zhang et al., 2012). However, this negative correlation might alternatively just reflect the decline of gammacerane-producing organisms under high salinities, as discussed above.

TS contents in lacustrine sediments are usually rather low and poorly correlate with TOC contents due to the low sulfate concentration in freshwater environments (Berner, 1984). The high TS values of the NR sediments (Figure 13A) further indicate high salinities. Negative correlations between TS and TIC (Figure 13B) might suggest that sulfate in the lake water was not or not entirely derived from carbonate weathering (e.g., from gypsum and anhydrite containing Keuper succession). TIC and thus carbonate contents are higher in the sediments of the marginal drilling, and the basal units B1 and A, i.e., in close proximity to the Jurassic carbonates. Alternatively, the negative correlation between TS and TIC could also result from the dilution of TS by rapid carbonate precipitation. The TIC content is likely to be controlled by water chemistry (in particular alkalinity), increasing the ionization of $H_2CO_3$ to

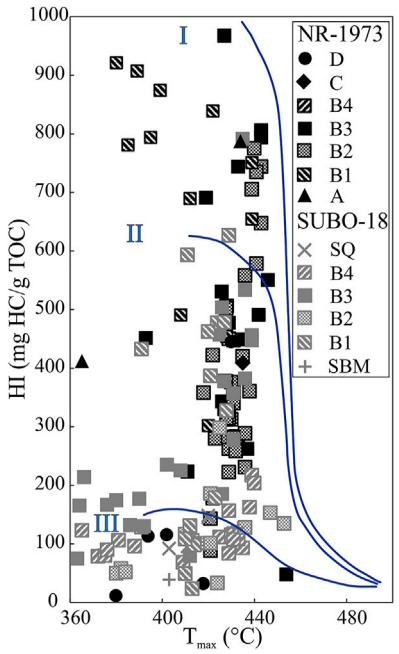


FIGURE 10
Rock-Eval HI vs $T_{max}$ plot indicating the kerogen type for the post-impact sediments in the Nördlinger Ries. See Figure 2 for stratigraphic units.

$CO_3^{2-}$ under alkaline conditions in the NR lake (Stüeken et al., 2020). In modern alkaline lakes, carbonate can precipitate rapidly near sources of $Ca^{2+}$, such as springs, and thus dilute other minerals and organic matter. The presence of travertine (porous limestone) mounds may support the inflow of $Ca^{2+}$-rich spring water that lasted at least 250 kyr (Arp et al., 2013). Therefore, the higher TIC levels in the marginal domain and the early central lake (unit A-B2) may reflect more favorable conditions for carbonate precipitation, such as a local source of $Ca^{2+}$ or elevated temperature leading to lower carbonate solubility.

Early investigations based on samples from the central drilling suggest that the depositional conditions evolved from playa lake (unit A) to alkaline-saline lake (unit B), then to a decreased salinity (unit C) and lately to freshwater conditions in unit D (Dehm et al., 1977; Füchtbauer and von der Brelie, 1977; Jankowski, 1977; Rothe and Hoefs, 1977; Jankowski, 1981), while a recent study on samples from the marginal site (SUBO-18) implied an evolution from alkaline fresh water conditions to a soda lake, followed by hypersaline conditions and finally the prevalence of karst water (Arp et al., 2014). It is worth noting that the salinity interpretation based on organic molecular tracers here represents a completely different approach (Figure 11), but also shows a trend from an initially intensively stratified mesosaline (A–B1) to the hypersaline lake with increasing water stratification (B2–B3), then gradually to lower, marine-like salinities with a less stratified water column (B4–C) towards unstratified fresh water in unit D after a short mesosalinity phase between units C and D, and finally back to weakly stratified normal marine-like water conditions at the top of unit D in the central lake. Units in the marginal domain correspondingly show the same trend but at lower water salinities and stratification levels.

### 5.3.3 Redox conditions and bio-productivity

Pr and Ph mainly originate from the phytol side chain of chlorophyll. The relative amount of Pr and Ph to their adjacent *n*-alkane as well as Pr/Ph can elucidate redox conditions, due to differential evolution pathways of their precursors in response to various redox conditions (Didyk et al., 1978; Hunt, 1995). However, other sources exist as well, in particular for phytane (ten Haven et al., 1987). Except for the coaly shale sample from borehole NR-1973 which is rather associated with oxic conditions based on high Pr/Ph and low Ph/*n*-$C_{18}$ values, all other samples are suggested to have formed under anoxic bottom water conditions showing high concentrations of Ph (Figures 6A, 7). Low Pr/Ph ratios over the two drilling profiles suggest anoxic conditions in the NR, while relatively high values for unit C and the coaly shale in unit D imply suboxic to oxic bottom water. Phytane can also be derived from halophilic archaea thriving in hypersaline water environments (ten Haven et al., 1987). Phytol within chlorophyll is more prone to be oxidized to pristane than the fully saturated phytanol side chains in halophilic archaea due to the occurrence of the double bond in the β-position of the hydroxyl group (Schinteie and Brocks, 2017). This factor might explain the high concentration of phytane and thus extraordinarily low Pr/Ph ratios in hypersaline settings such as NR (ten Haven et al., 1987; Jahnke et al., 2008). Independent of the precursor, low Pr/Ph can still be regarded as an excellent indicator of anoxic bottom water conditions (ten Haven et al., 1987).

The crossplot for the gammacerane index vs Pr/Ph (Supplementary Appendix Figure A1) shows no link between the two parameters, as found for other lacustrine sediments (e.g., Zhao et al., 2021). It should be noted that microscopic observations do not extensively show fine lamination as typical of microbial mats or mats made up of photosynthetic organisms; these may change the oxygen level at the sediment/water interface (Pawlowska et al., 2013). Aryl isoprenoids, which can reflect photic zone euxinia, have not been detected in the analyzed samples. The occurrence of des-A-lupane in the analyzed samples, which is reported to be formed by degradation of lupane under anoxic conditions (Trendel et al., 1989), in combination with the presence of small pyrite framboids (mostly <5 μm) further supports anoxic bottom water conditions (Wilkin et al., 1996).

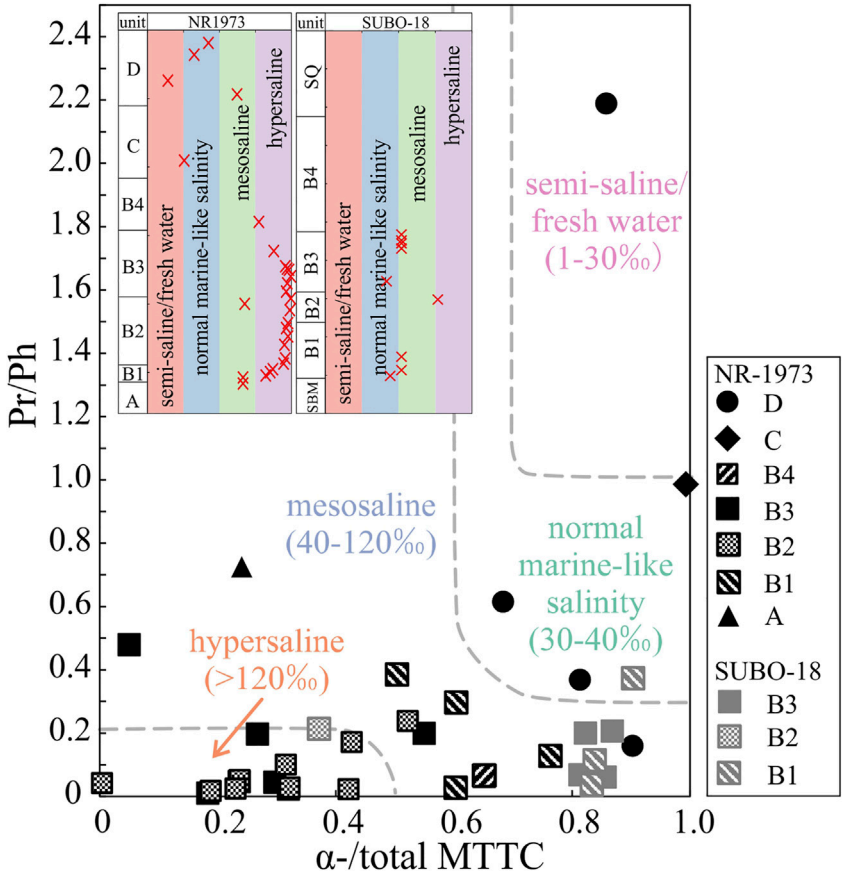


FIGURE 11
Crossplot of α-/total MTTC vs Pr/Ph of the post-impact sediments in the Nördlinger Ries (modified after Schwark et al., 1998; Wang et al., 2011; Jiang et al., 2019). See Figure 2 for stratigraphic units.

Homohop-17 (21)-enes clearly exhibit an increasing concentration from $C_{31}$ to $C_{35}$ in the lower part of the central profile with high values of $C_{35}/C_{31\text{-}35}$ homohop-17 (21)-enes (Table 2). Higher values of $C_{35}/C_{31\text{-}35}$ homohop-17 (21)-enes in borehole NR-1973 compared to SUBO-18 demonstrate intense water anoxicity in the central lake as compared to the margin. To summarize, anoxic depositional conditions prevailed over almost all the investigated periods in the center and at the margin of the NR, except for unit C and the period represented by the coaly shale in unit D in the central crater, when suboxic conditions may have prevailed (Figure 6A and Supplementary Appendix Figure A1). Anoxic bottom water is also indicated by the quasi absence of hopanes representing aerobic bacteria in units B2 and B3 as evident from the very high sterane/hopane ratios (Table 2).

Reducing bottom water in the NR is the dominant factor controlling the OM preservation as illustrated by Pr/Ph ratios <1. Furthermore, there seems to be a very rough trend of increasing TOC contents with decreasing Pr/Ph ratios (Figure 14).

## 5.4 Ecological evolution

A clue on past bio-communities can be obtained from the composition and relevant ratios of normal alkanes. Most of the central samples are dominated by short-chain *n*-alkanes (*n*-$C_{15\text{-}19}$, Table 2 and Figure 5B), suggesting major OM input from microorganisms and algae (Cranwell, 1977), which is in agreement with high ($n$-$C_{15}$+$n$-$C_{17}$)/($n$-$C_{23}$+$n$-$C_{25}$) values, high Paq values (>0.4, Ficken et al., 2000; Table 2 and Figure 6A) as well as low terrigenous/aquatic ratios (TAR, Meyers, 1997; Figure 6A). This is further supported by the high concentrations of short-chain *n*-alkanoic fatty acids and esters (Table 3), which are the precursory compounds for alkanes as they lose ester/carboxylic groups upon diagenesis, especially considering that total amenable fatty acids account for 10–57% (Barakat and Rullkötter, 1995b) of the total heteroatomic fraction (more than 65 weight-% of the total extracts; Rullkötter et al., 1990). The predominance of $C_{16}$ *n*-alkanoic acid further indicates an algal OM source in productive lakes (Cranwell et al., 1987). These results are in agreement with the petrological

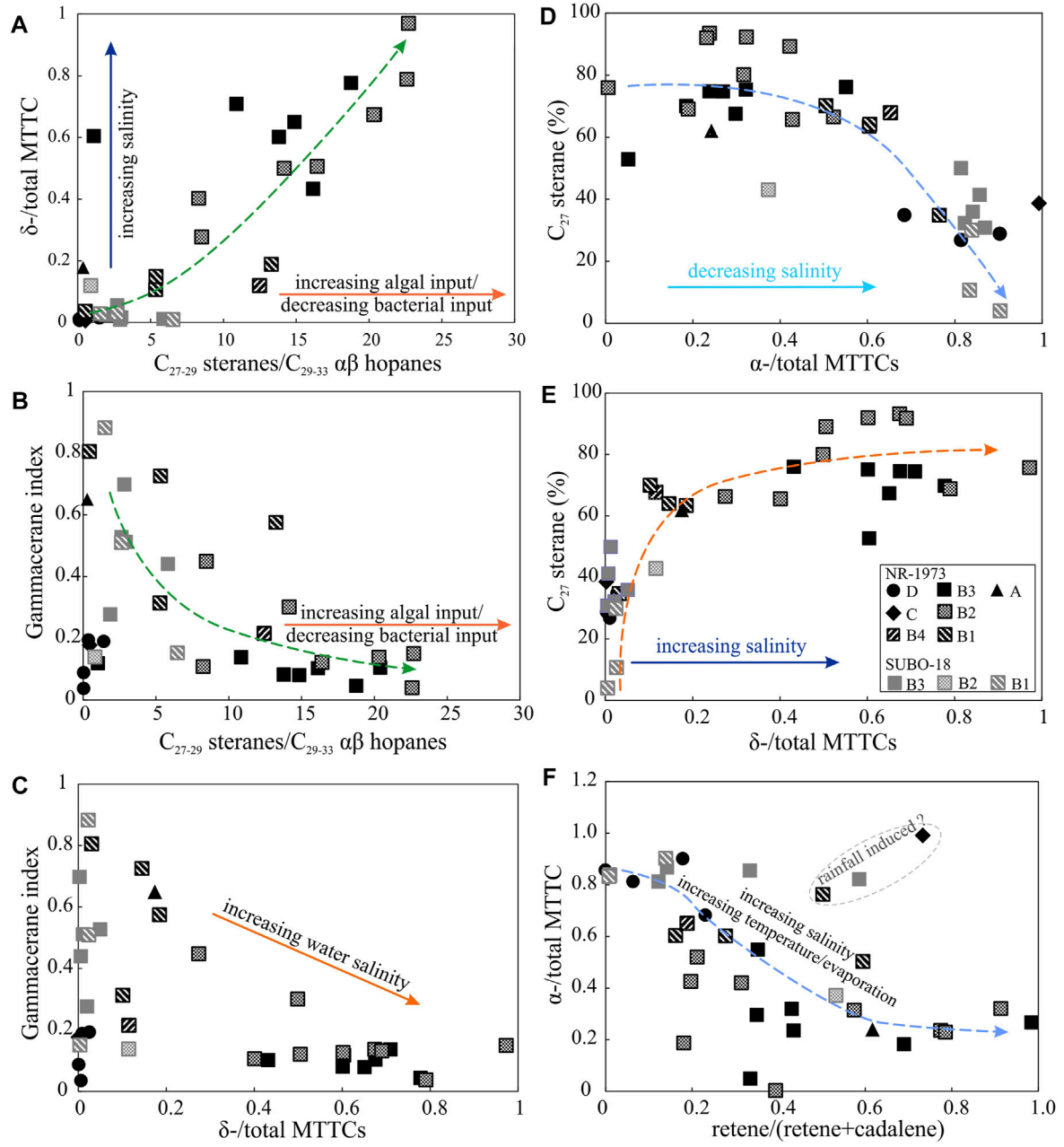


FIGURE 12
Relations between paleo-climate, water salinities and bio-communities. **(A)** δ-/total MTTC vs $C_{27-29}$ steranes/$C_{29-33}$ αβ hopanes, **(B)** gammacerane index (gammacerane/(gammacerane+$C_{30}$ αβ hopane)) vs $C_{27-29}$ steranes/$C_{29-33}$ αβ hopanes, **(C)** gammacerane index vs δ-/total MTTC **(D,E)** $C_{27}$ sterane relative percentage vs α-/total MTTC and δ-/total MTTC, **(F)** α-/total MTTC vs retene/(retene+cadalene). See text for discussion of these biomarker ratios. See Figure 2 for stratigraphic units.

observations (rare vitrinite and inertinite; Figure 9). The uppermost coaly shale in the center and samples from the marginal borehole show higher concentration of long-chain *n*-alkanes and higher TAR values, while Paq values are low (~0.2), indicating a contribution of vascular higher land plants to the OM (Eglinton and Hamilton, 1967; Figures 5, 6A). The limited terrigenous OM input to the sediments during most of the depositional phases (units B–C, except the marginal lowermost B1) may be explained by limited fluvial supply from the rim around the crater lake.

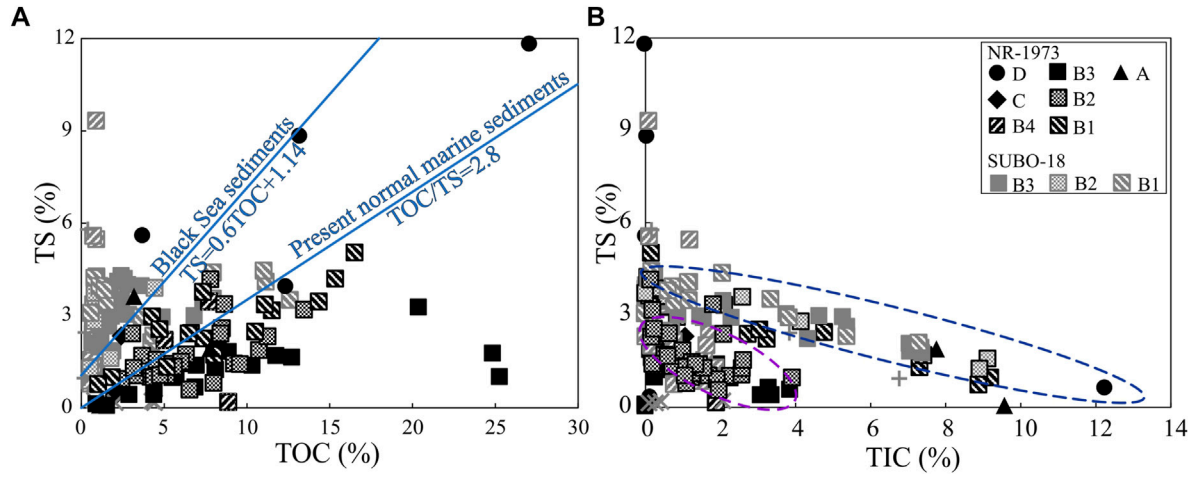


FIGURE 13
Crossplots of TS vs **(A)** TOC and **(B)** TIC of the post-impact sediments in the Nördlinger Ries. TS=total sulphur content, TOC=total organic carbon content, TIC=total inorganic carbon content. See Figure 2 for stratigraphic units.

Ratios of DTPs/$C_{30}$ αβ hopane and DTPs/$C_{27}$ steranes show a weak increase up the section in the two studied boreholes, but stay at low values in the lower-middle sequence of the NR (i.e., units A–C in borehole NR-1973, and units B1–B3 in borehole SUBO-18), while they significantly increase in the upper succession (unit D in the NR-1973), with DTPs/C30 αβ hopane ratio peaking in the coaly shale sample (Table 2; Figures 6B,C), in which $C_{27}$ steranes are almost absent. This observation further supports that higher land plants contributed a negligible portion to OM during most of the evolution of the NR, while they became the primary contributor during deposition of unit D (Figure 6C). The presence of coaly shales suggests a temporarily swampy environment, at least in some shallow water parts of the lake in its final stage. Such a stage leads to the release of humic acids into the lake water; thus the alkaline lake ultimately turned into a neutral or even slightly acidic stage.

The sparse occurrence of vitrinite/inertinite together with the TAR, Paq and DTPs indices in the examined samples of SUBO-18 imply that higher land plants contributed more to OM in the marginal domain than in the center, but still to only a small extent as compared to algae and microbes. The lowermost unit B1 at the margin (the very initial marginal phase of the lake), contains abundant vitrinite/inertinite particles and higher abundance of long-chain *n*-alkanes, higher TAR, and low Paq values suggesting abundant land plant contribution to OM in the initial marginal lake (Table 2; Figures 6A–C).

Pertaining to the species of higher land plants, high values of retene/(retene+cadalene) imply the thriving of drought-tolerant plants (see *Section 5.3.1*) in middle B2 and lower B3 units (Figure 6B). 4β(H)-19-norisopimarane, 16α(H)-phyllocladane, ent-16α(H)-kaurane and retene found in the analyzed samples are all reported to originate from gymnosperms (Noble et al., 1986; Simoneit et al., 1986), while des-A-lupane is formed by degradation of lupane from angiosperms (Trendel et al., 1989). The ratio of des-A-lupane/DTPs is generally low (Table 2), suggesting dominant gymnosperm input. The absence of oleanane in the samples further proves the low contribution of angiosperms. Given the morphology of the crater, and the absence of fluvial input, the higher land plant particles in the post-impact sediments are assumed to be airborne and of allochthonous origin beyond the crater rim. In contrast, the abundant higher land plant fragments in unit D should be autochthonic due to the occurrence of more favorable, very shallow water conditions. Higher land plants in the lowermost unit B1 (sample 20/374) at the margin may be of allochthonous origin as well.

$C_{27}$ steranes are the main steranes in red algae species (Huang and Meinschein, 1979; Mackenzie et al., 1982; Volkman, 1986; Kodner et al., 2008), and the $C_{27\text{-}29}$ steranes/$C_{30\text{-}31}$ αβ hopanes ratio implies the contribution of eukaryotes (e.g., algae, Kodner et al., 2008) vs prokaryotes (i.e., aerobic bacteria, Rohmer et al., 1984) to OM. Accordingly, the number of eukaryotes shows a first drastic increase from unit A to middle B2 then maintained on a high level until a decrease occurred during stage D, with unit B clearly being dominated presumably by red algae ($C_{27}$ steranes up to 97%; Figures 6C, 8), which would be in line with the findings of Rhodophyceae fossils reported by Dehm et al. (1977) and Füchtbauer and von der Brelie (1977) in the NR sediments. Units A and C might, however, show a significant contribution of prokaryotic species to OM indicated by relatively low values of the $C_{27\text{-}29}$ steranes/$C_{30\text{-}31}$ αβ hopane. For the marginal area, the relative contribution of eukaryotes to OM is constant but lower than in the central domain (NR-1973). Here, higher land plants contributed more to

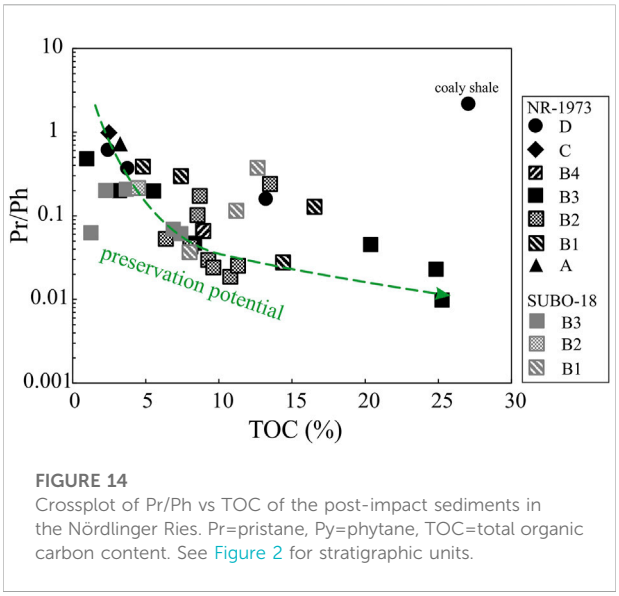


FIGURE 14
Crossplot of Pr/Ph vs TOC of the post-impact sediments in the Nördlinger Ries. Pr=pristane, Py=phytane, TOC=total organic carbon content. See Figure 2 for stratigraphic units.

OM in the lowermost unit B1 (Figure 6C), and then diatoms/bryophytes bloomed in upper B1 with increasing $C_{28}$ steranes (Figure 8; Volkman, 1986). From unit B2 to B3, the $C_{27}$ sterane (%) plot (Figure 6C) indicates that red algae gradually increased, but their abundance is generally lower than in the central domain. The thrive of red algae species in the Miocene alkaline NR-lake might correspond to similar observations on modern alkaline lakes, such as Lake Natron, in Tanzania (Brown, 1955).

The prominent amount of microscopically visible unstructured fluorescing groundmass (UFG) in most of the examined samples may be explained by 1) a lack of resistant cell macromolecules (e.g., algaenan in green algae) resulting in the formation of UFG upon diagenesis (Largeau and Derenne, 1993) or 2) early diagenetic vulcanization processes, which destroyed the morphology of OM (Taylor et al., 1998). High percentages of $C_{27}$ steranes might reflect a rather restricted biodiversity under highly saline and alkaline conditions. The covariation trend between δ-/total MTTC and $C_{27-29}$ steranes/$C_{29-32}$ αβ hopane points to the prevalence of algae but withered bacterial species in the biocommunities (Figure 12A). The correlations between $C_{27}$ steranes and δ-/total MTTC and α-/total MTTC, respectively, might imply that the $C_{27}$ steranes mainly originate from halophilic red algae (Figures 12D,E), which is in line with the conclusions made by Füchtbauer and von der Brelie (1977) and Dehm et al. (1977). Hopanoids mainly originate from aerobic bacteria (Farrimond et al., 1998; Brocks and Summons, 2004) while they are less commonly produced by anaerobic species (Fischer et al., 2005). The rare occurrence of hopanoids corroborates with the anoxic conditions (with extraordinarily low Pr/Ph values) and high $C_{27-29}$ steranes/$C_{29-32}$ αβ hopane ratios in the studied samples. This further reinforces the intense anoxic conditions through most parts of the water column and the decay of aerobic bacteria inhabiting zones above chemocline in the water column.

Although monomethyl alkanes, which were found to be abundant in cultured and natural communities of cyanobacteria (e.g., Shiea et al., 1990), were only found in samples of units A, C and D in the central well (NR-1973), and at the bottom B3 in the marginal lake (SUBO-18). The *iso*- and *anteiso*-esters and fatty acids present in all the measured samples, including unit B, may imply the occurrence of cyanobacteria over all the evolutional stages of the NR. In summary, there might be evidence that cyanobacteria developed during some stages in the NR lake based on the presence of monomethyl alkyl compounds, while the absence of 2α-methylhopane and monomethylated alkanes make the occurrence of cyanobacteria enigmatic in unit B. For the marginal units, cyanobacterial mats cannot be excluded, due to the occurrence of stromatolites and bioherms in the marginal setting (Arp et al., 2014).

Variations of $\delta^{13}C$ provide insights into the biological precursor material of Pr and Ph (Table 3). Ph in this study is isotopically heavier (enriched in $^{13}C$) than Pr. Values observed are significantly lower than Pr and Ph isotope values assigned to halophilic archaea (Grice et al., 1998b, $\delta^{13}C$ ca. −17–−14‰), or algae from within a $CO_2$-limited ecosystem (Schouten et al., 2001, $\delta^{13}C$ ca. −17‰). Pr in this study is isotopically lighter than Pr in Miocene marine sediments (Pagani et al., 2000, ca. −30.5‰). Pr is mostly depleted in $^{13}C$ by 4–7‰ compared to Ph in this study, potentially implying a second source for phytane in addition to chlorophyll (Volkman et al., 2015). Simultaneously, intramolecular carbon isotope fractionation might enhance the depletion of $^{13}C$ in pristane relative to phytane during deposition (Schouten et al., 2008).

As discussed above, extremely low values of Pr/Ph in sediments deposited under hypersaline conditions can be attributed to the contribution of halophilic archaea to Ph (ten Haven et al., 1987). $^{13}C$-rich phytanyl from archaea derived lipids is a potential source for isotopically heavy phytane leading to a positive shift of $\delta^{13}C$ as compared to pristane (Rowland, 1990; Rowland and Robson, 1990; Grice et al., 1998b). It is worth noting that samples 18/723 (unit B3), 18/740 and 18/756 (unit B2), having low α-/total MTTC values (suggesting high salinities), are characterized by quite similar $\delta^{13}C$ values of Pr and Ph, indicating that the two isoprenoids have the same precursor, e.g., halophilic algae. The obtained $\delta^{13}C$ values for $C_{27}$ steranes in samples representing high saline conditions (i.e., samples 18/756 and 18,761; Table 3) are quite similar to those reported for other Miocene hypersaline environments with major OM input from algae and/or cyanobacteria (Grice et al., 1998a, $\delta^{13}C$ −26.5–−26.3‰). However, they are much more negative than those reported for Miocene deposits of algal origin in a $CO_2$-limited ecosystem (Schouten et al., 2001, $\delta^{13}C$ −17.7–−16.6‰). The occurrence of non-$CO_2$-limited

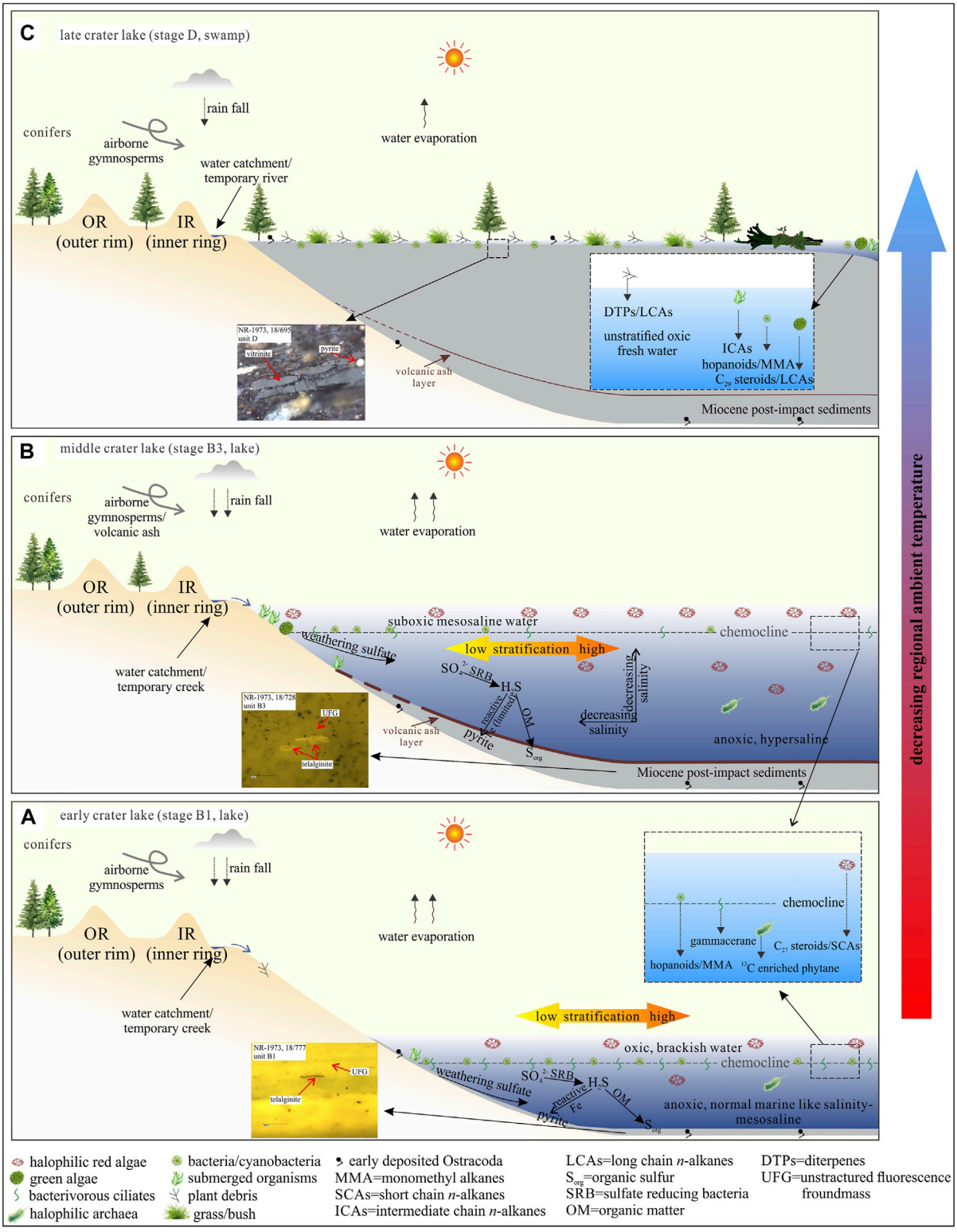


FIGURE 15
Evolutionary model of the paleo Nördlinger Ries lake. **(A)** Early crater lake, **(B)** middle crater lake, **(C)** late crater lake phase. Stages B1, B3 and D refer to stratigraphic units in Figure 2. OR=outer rim, IR=inner ring. Paleontology follows Arp et al. (2014).

ecosystems is therefore assumed in the NR lake over its evolutionary stages.

Methanogens can survive in sulfate-rich hypersaline environments, while they flourish within sulfate-depleted sediments (Wilms et al., 2007; McGenity and Sorokin, 2010). The rare occurrence of 2,6,10,15,19-pentamethylicosane (PMI) in the studied samples implies a limited methanogenesis intensity (Summons et al., 1998; Boetius et al., 2000; Birgel et al., 2008), which is in accordance with the inferred sulfate-rich, hypersaline NR lake water.

In the central domain, halophilic red algae/plankton and aerobic bacteria prevailed during the deposition of units A, B1 and C, while units B2 and B3 were dominated by halophilic red algae/plankton (Figures 5, 6C, 8). Sterane/hopane ratios are very high there, 10 to 100 times higher than in units A and C and also much higher than reported for most petroleum source rocks (e.g., Wang et al., 2021; Xia et al., 2021; Zhao et al., 2021) indicating that aerobic bacteria were almost absent. Autochthonous drought-tolerant gymnosperms became the major plant species during the deposition of unit D (Figures 6B,C). At the crater's margin, such species contributed to OM to a comparably higher extent, especially in lowermost unit B1, showing higher amounts of diterpenoids and $C_{29}$ steranes compared to the central unit B (Figures 6B,C, 8). From the upper part of unit B1 on, the marginal bio-community was controlled by autochthonous algae, i.e., green algae in unit B1, and halophilic red algae/plankton in units B2 and B3 (Figure 8). Halophilic archaea contributed to OM over the whole evolutionary stage of the Ries lake. Cyanobacteria developed in the NR, but their occurrence and abundance are not clearly confirmed for unit B. Methanogens were rather inactive in response to the sulfate-rich hypersaline environment.

## 5.5 Implications on crater lake evolution

As discussed above, rainfall was the main fresh water supply to the lake. However, a semi-arid climate prevailed during the Miocene in southern Germany (Jankowski, 1981), thus limiting the freshwater input to the lake. Together with higher paleo-temperature, this probably enhanced evaporation and caused increasing water salinity from the early stage (Figures 12F, 15A) to mid stage (Figure 15B) of the lake. Chemical weathering of the catchment area was another factor controlling the chemical evolvement of the NR lake (Arp et al., 2014), which is also related to paleo-temperature and precipitation. Given the hydrologically closed lake setting, salts (e.g., sulfate) in the lake water might have been derived from weathering products of the nearby rocks inside the outer rim (Figures 15A,B), or partly from the springs near the lake margin (Arp et al., 2013). It is worthwhile noting that gypsum is present in the Triassic lower and middle Keuper successions (Mujal and Schoch, 2020). Bunte breccia containing Keuper fragments was previously recorded in the NR (Füchtbauer and von der Brelie, 1977) and this Triassic sequence might be a possible source for the sulfate in the post-impact lake water and thus the TS in the sediments.

Intense water column stratification and anoxic bottom water conditions are inevitably caused by high water salinities and decomposition of OM. Over most of the deposition time of the NR sediments (Figures 15A,B), the anoxic bottom water in an alkaline lake with high salinities was not disturbed as indicated by consistently low Pr/Ph ratios until the late lake stage D. An outlet was reported to have formed during this latest stage (Jankowski, 1977), through which saline water was pushed out of the lake by incoming freshwater, resulting in a change of the overall setting towards oxic or suboxic conditions indicated by high Pr/Ph ratios (unit D, Figure 15C).

Elevated $\delta^{15}N$ values reported by Stüeken et al. (2020) can be induced by both evaporation of ammonia (Stüeken et al., 2016; Deng et al., 2018) and biological redox processes (e.g., denitrification) of the alkaline lacustrine sediments (Cao et al., 2020; Stüeken et al., 2020), while bacterial nitrification and denitrification stop when the water salinity exceeds 35‰ (Cao et al., 2020). Considering the high water salinity in the NR (salinity mostly over 40‰, Figure 11), ammonia volatilization might be the main reason for the positive shift of $\delta^{15}N$ values presented by Stüeken et al. (2020) for units A–C. During the early depositional phase of unit D, the water salinity apparently decreased, and the weakening ammonia volatilization together with bacterial denitrification shifted $\delta^{15}N$ to lower but still positive values compared to the early stage of the NR lake.

Restricted bio-communities in such lake systems develop in response to the harsh water chemistry. Anoxic, hypersaline and alkaline lakes are commonly eutrophic (Xia et al., 2021). The ratio of halophilic algal species over prokaryotes is often high, as in the case of the early-middle NR lake, meaning the lake was highly bio-productive with little contribution from aerobic bacteria, cyanobacteria and methanotrophic bacteria to OM (Figures 15A,B). During the swampy stage D (Figure 15C), higher land plants dominated the bio-community and thus the contribution to OM. Thermodynamic transformation of microbial $H_2S$ to $HS^-$ and $S^{2-}$ under alkaline conditions can be significantly enhanced, which might have favored the incorporation of sulfur into OM in an iron-poor environment in the NR. This process probably led to the formation of abundant organic sulfur-rich kerogen in the NR (Rullkötter et al., 1990).

# 6 Conclusion

Previous studies on large and representative sample sets from the Nördlinger Ries lake sediments mainly focused on results from

inorganic and isotope geochemistry, mineralogy and sedimentology. Molecular organic geochemistry studies focused on just a few samples and thus not on the evolution of the lake. This study systemically applies organic geochemistry and organic petrology data measured on a large number of samples through one central and one more marginal lake sediment profile. Chemostratigraphy and detailed kerogen typing through the profiles are presented for the first time based on bulk geochemistry and Rock-Eval parameters. Previous assumptions on salinity and redox condition trends are now compared to those derived from biomarker parameters. Furthermore, the dominant primary bio-producers in the evolving alkaline lake were deduced from molecular geochemistry data for the first time. In detail, the following conclusions can be drawn:

1) Based on Rock-Eval pyrolysis data, kerogen in the center mainly consists of type I or type II kerogen, whereas the marginal sequence is mainly composed of type II-III kerogen. Mineral matrix effects are expected due to the presence of abundant illite and smectite as well as zeolites, causing an underestimation of kerogen quality.
2) Water salinity is assumed to control water stratification in the paleo-lake, with stronger stratification levels in the lake center than at the margin. Hypersaline water prevailed since the early lake stage until unit B4 in the center, and then decreased to normal marine-like salinity with a short step back to mesosaline conditions at the border of units C and D, and finally to freshwater during the coaly shale deposition. The investigated marginal site shows similar variations compared to the lake center, but at lower, mesosaline levels. Based on Pr/Ph ratios anoxic bottom water prevailed in the paleo-lake during most of its history, while conditions became more oxygenated during deposition of the uppermost Miocene units C and D.
3) Autochthonic halophilic red algae/plankton, cyanobacteria and aerobic bacteria prevailed during the deposition of units A and C, while unit B was dominated by halophilic red algae/plankton in the central lake. Significant amounts of higher land plant-derived organic matter are only present in unit D.
4) Water salinities were largely controlled by semi-arid, warm paleo-climate and rock chemistry in the area adjacent to the impact crater. The transformation of dissolved $H_2S$ to $HS^-/S^{2-}$ was boosted by the alkaline conditions, and–in the absence of much iron–enhanced the vulcanization of OM.

## Data availability statement

The datasets generated during and/or analysed during the current study are available from the corresponding author on reasonable request.

## Author contributions

ZZ performed most of the laboratory work, data interpretation and wrote the first draft of the MS. SG wrote sections of the MS and helped in constructing the final draft. LZ wrote sections of the MS and helped in constructing the final draft. WD helped with the laboratory work. RL helped wirth data interpretation and checked and approved the final draft. All authors contributed to manuscript revision, read, and approved the submitted version.

## Acknowledgments

The authors would like to thank Jan Schwarzbauer, Alireza Baniasad, Donka Macherey, Annette Schneiderwind as well as Kerstin Windeck for their technical assistance during the study. We thank Dietmar Jung at Bavarian Environment Agency for providing samples of the marginal drilling. We thank reviewers Kai Mangelsdorf at German Research Centre for Geosciences (GFZ) Potsdam, Germany, Assoc. Doaa Mousa at Egyptian Petroleum Research Institute Cairo, Egypt, and Assoc. NE, Helwan University, Egypt for their constructive comments which helped to improve the quality of this paper. We thank Assoc. AD from the Faculty of Science, Assiut University, Egypt, for handling our manuscript.

## Conflict of interest

The authors declare that the research was conducted in the absence of any commercial or financial relationships that could be construed as a potential conflict of interest.

## Publisher's note



## Supplementary material

The Supplementary Material for this article can be found online at: https://www.frontiersin.org/articles/10.3389/feart.2022.989478/full#supplementary-material

# References


Arp, G., Blumenberg, M., Hansen, B. T., Jung, D., Kolepka, C., Lenz, O., et al. (2014). Chemical and ecological evolution of the Miocene Ries impact crater lake, Germany: A reinterpretation based on the enkingen (SUBO 18) drill core. *Geol. Soc. Am. Bull.* 125, 1125–1145. doi:10.1130/b30731.1

Arp, G., Dunkl, I., Jung, D., Karius, V., Lukács, R., Zeng, L., et al. (2021). A volcanic ash layer in the Nördlinger Ries impact structure (Miocene, Germany): Indication of crater fill geometry and origins of long-term crater floor sagging. *JGR. Planets* 126, e2020JE006764. doi:10.1029/2020je006764

Arp, G., Hansen, B. T., Pack, A., Reimer, A., Schmidt, B. C., Simon, K., et al. (2017). The soda lake—Mesosaline halite lake transition in the Ries impact crater basin (drilling löpsingen 2012, Miocene, southern Germany). *Facies* 63, 1–20. doi:10.1007/s10347-016-0483-7

Arp, G., Kolepka, C., Simon, K., Karius, V., Nolte, N., and Hansen, B. T. (2013). New evidence for persistent impact-generated hydrothermal activity in the Miocene Ries impact structure, Germany. *Meteorit. Planet. Sci.* 48, 2491–2516. doi:10.1111/maps.12235

Arp, G., Reimer, A., Simon, K., Sturm, S., Wilk, J., Kruppa, C., et al. (2019). The Erbisberg drilling 2011: Implications for the structure and postimpact evolution of the inner ring of the Ries impact crater. *Meteorit. Planet. Sci.* 54, 2448–2482. doi:10.1111/maps.13293

Bader, K., and Schmidt-Kaler, H. (1990). Talausbildung vor und nach dem Impakt im Trümmermassengebiet des östlichen Riesvorlandes. *Mitt. Geogr. Ges. München* 75, 31–36.

Barakat, A. O., Baumgart, S., Brocks, P., Scholz-Böttcher, B. M., and Rullkötter, J. (2012). Alkylated phenol series in lacustrine black shales from the Nördlinger Ries, southern Germany. *J. Mass Spectrom.* 47, 987–994. doi:10.1002/jms.3049

Barakat, A. O., Peakman, T. M., and Rullkötter, J. (1994). Isolation and structural characterization of 10-oxo-octadecanoic acid in some lacustrine sediments from the Nördlinger Ries (southern Germany). *Org. Geochem.* 21, 841–847. doi:10.1016/0146-6380(94)90043-4

Barakat, A. O., and Rullkötter, J. (1997). A comparative study of molecular paleosalinity indicators: Chromans, tocopherols and C20 isoprenoid thiophenes in Miocene lake sediments (nördlinger Ries, southern Germany). *Aquat. Geochem.* 3, 169–190.

Barakat, A. O., and Rullkötter, J. (1995b). Extractable and bound fatty acids in core sediments from the Nördlinger Ries, southern Germany. *Fuel* 74, 416–425. doi:10.1016/0016-2361(95)93476-t

Barakat, A. O., and Rullkötter, J. (1994a). Free aliphatic acids in sulfur-rich lacustrine sediments: Their origin and relation to hydrocarbons. *Energy fuels.* 8, 474–480. doi:10.1021/ef00044a028

Barakat, A. O., and Rullkötter, J. (1994b). Occurrence and identification of $C_{33}$, $C_{37}$, and $C_{38}$ organic sulfur compounds in sediment extracts. *Energy fuels.* 8, 1168–1174. doi:10.1021/ef00048a002

Barakat, A. O., and Rullkötter, J. (1999). Origin of organic sulfur compounds in sediments from the Nördlinger Ries (southern Germany). *J. Pet. Sci. Eng.* 22, 103–119. doi:10.1016/s0920-4105(98)00060-6

Barakat, A. O., and Rullkötter, J. (1995a). *The distribution of free organic sulfur compounds in sediments from the Nördlinger Ries, Southern Germany*. Washington, DC: American Chemical Society, 311–331.

Barakat, A. O., Scholz-Böttcher, B. M., and Rullkötter, J. (2013). Lipids in a sulfur-rich lacustrine sediment from the N∫ouml;rdlinger Ries (southern Germany) with a focus on free and bound sterols. *Geochem. J.* 47, 397–407. doi:10.2343/geochemj.2.0258

Behar, F., Beaumont, V., and Penteado, H. D. B. (2001). Rock-eval 6 technology: Performances and developments. *Oil Gas Sci. Technol. -. Rev. IFP.* 56, 111–134. doi:10.2516/ogst:2001013

Berner, R. A. (1984). Sedimentary pyrite formation: An update. *Geochim. Cosmochim. Acta* 48, 605–615. doi:10.1016/0016-7037(84)90089-9

Birgel, D., Himmler, T., Freiwald, A., and Peckmann, J. (2008). A new constraint on the antiquity of anaerobic oxidation of methane: Late Pennsylvanian seep limestones from southern Namibia. *Geol.* 36, 543–546. doi:10.1130/g24690a.1

Boetius, A., Ravenschlag, K., Schubert, C. J., Rickert, D., Widdel, F., Gieseke, A., et al. (2000). A marine microbial consortium apparently mediating anaerobic oxidation of methane. *Nature* 407, 623–626. doi:10.1038/35036572

Bourbonniere, R. A., and Meyers, P. A. (1996). Anthropogenic influences on hydrocarbon contents of sediments deposited in eastern Lake Ontario since 1800. *Environ. Geol.* 28, 22–28. doi:10.1007/s002540050074

Bray, E., and Evans, E. (1961). Distribution of n-paraffins as a clue to recognition of source beds. *Geochim. Cosmochim. Acta* 22, 2–15. doi:10.1016/0016-7037(61)90069-2

Brocks, J., and Summons, R. (2004). in *Sedimentary hydrocarbons, biomarkers for early life. Biogeochemistry, Treatise on Geochemistry*. Editors H. D. Holland and K. K. Turekian (Amsterdam: Elsevier), 64–115.

Brown, L. H. (1955). The breeding of lesser and greater flamingoes in East Africa. *J. East Afr. Nat. Hist.* 22, 159–162.

Buchner, E., Schwarz, W. H., Schmieder, M., and Trieloff, M. (2010). Establishing a 14.6±0.2 Ma age for the nördlinger Ries impact (Germany)—a prime example for concordant isotopic ages from various dating materials. *Meteorit. Planet. Sci.* 45, 662–674. doi:10.1111/j.1945-5100.2010.01046.x

Cao, J., Xia, L., Wang, T., Zhi, D., Tang, Y., and Li, W. (2020). An alkaline lake in the late paleozoic ice age (lpia): A review and new insights into paleoenvironment and petroleum geology. *Earth. Sci. Rev.* 202, 103091. doi:10.1016/j.earscirev.2020.103091

Christ, N., Maerz, S., Kutschera, E., Kwiecien, O., and Mutti, M. (2018). Palaeoenvironmental and diagenetic reconstruction of a closed-lacustrine carbonate system–the challenging marginal setting of the Miocene Ries Crater Lake (Germany). *Sedimentology* 65, 235–262. doi:10.1111/sed.12401

Cranwell, P., Eglinton, G., and Robinson, N. (1987). Lipids of aquatic organisms as potential contributors to lacustrine sediments—II. *Org. Geochem.* 11, 513–527. doi:10.1016/0146-6380(87)90007-6

Cranwell, P. (1977). Organic geochemistry of cam loch (sutherland) sediments. *Chem. Geol.* 20, 205–221. doi:10.1016/0009-2541(77)90044-4

Dehm, R., Gall, H., Höfling, R., Jung, W., and Malz, H. (1977). Die Tier- und Pflanzenreste aus den obermiozänen Riessee-Ablagerungen in der Forschungsbohrung Nördlingen 1973. *Geol. Bavarica* 75, 91–111.

Deng, Y., Li, Y., and Li, L. (2018). Experimental investigation of nitrogen isotopic effects associated with ammonia degassing at 0–70° C. *Geochim. Cosmochim. Acta* 226, 182–191. doi:10.1016/j.gca.2018.02.007

Didyk, B., Simoneit, B., Brassell, S. t., and Eglinton, G. (1978). Organic geochemical indicators of palaeoenvironmental conditions of sedimentation. *Nature* 272, 216–222. doi:10.1038/272216a0

dos Santos Neto, E. V., Hayes, J. M., and Takaki, T. (1998). Isotopic biogeochemistry of the neocomian lacustrine and upper aptian marine-evaporitic sediments of the potiguar basin, northeastern Brazil. *Org. Geochem.* 28, 361–381. doi:10.1016/s0146-6380(98)00007-2

Eglinton, G., and Hamilton, R. J. (1967). Leaf epicuticular waxes. *Science* 156, 1322–1335. doi:10.1126/science.156.3780.1322

Erickson, T. M., Pearce, M. A., Reddy, S. M., Timms, N. E., Cavosie, A. J., Bourdet, J., et al. (2017). Microstructural constraints on the mechanisms of the transformation to reidite in naturally shocked zircon. *Contrib. Mineral. Pet.* 172, 6. doi:10.1007/s00410-016-1322-0

Espitalié, J., Deroo, G., and Marquis, F. (1985). La pyrolyse Rock-Eval et ses applications. Deuxième partie. *Rev. Inst. Fr. Pet.* 40, 755–784. doi:10.2516/ogst:1985045

Farrimond, P., Fox, P., Innes, H., Miskin, I., and Head, I. (1998). Bacterial sources of hopanoids in recent sediments: Improving our understanding of ancient hopane biomarkers. *Anc. Biomol.* 2, 147–166.

Ficken, K. J., Li, B., Swain, D., and Eglinton, G. (2000). An *n*-alkane proxy for the sedimentary input of submerged/floating freshwater aquatic macrophytes. *Org. Geochem.* 31, 745–749. doi:10.1016/s0146-6380(00)00081-4

Fischer, W., Summons, R., and Pearson, A. (2005). Targeted genomic detection of biosynthetic pathways: Anaerobic production of hopanoid biomarkers by a common sedimentary microbe. *Geobiology* 3, 33–40. doi:10.1111/j.1472-4669.2005.00041.x

Füchtbauer, H., and von der Brelie, G. (1977). *Tertiary lake sediments of the Ries, research borehole noerdlingen 1973-A summary*, 75. Munich: Geologica Bavarica, 13–19.

Grice, K., Schouten, S., Nissenbaum, A., Charrach, J., and Sinninghe Damsté, J. S. (1998a). A remarkable paradox: Sulfurised freshwater algal (*Botryococcus braunii*) lipids in an ancient hypersaline euxinic ecosystem. *Org. Geochem.* 28, 195–216. doi:10.1016/s0146-6380(97)00127-7

Grice, K., Schouten, S., Nissenbaum, A., Charrach, J., and Sinninghe Damsté, J. S. (1998b). Isotopically heavy carbon in the $C_{21}$ to $C_{25}$ regular isoprenoids in halite-rich deposits from the Sdom Formation, Dead Sea Basin. *Org. Geochem.* 28, 349–359. doi:10.1016/s0146-6380(98)00006-0

Hammer, U. T. (1981). "Primary production in saline lakes," in *Salt lakes* (Dordrecht: Springer), 47–57.

Hörz, F., Ostertag, R., and Rainey, D. (1983). Bunte Breccia of the Ries: Continuous deposits of large impact craters. *Rev. Geophys.* 21, 1667–1725. doi:10.1029/rg021i008p01667

Huang, W.-Y., and Meinschein, W. (1979). Sterols as ecological indicators. *Geochim. Cosmochim. Acta* 43, 739–745. doi:10.1016/0016-7037(79)90257-6

Hunt, J. M. (1995). *Petroleum geochemistry and geology*. New York: W. H. Freeman.

Hüttner, R., and Schmidt-Kaler, H. (1999). *Die Geologische Karte des Rieses 1: 50000: Erläuterungen zu Erdgeschichte, Bau und Entstehung des Kraters sowie zu den Impaktgesteinen*, 104. Munich: Geologica Bavarica, 7–76.

Jahnke, L., Orphan, V., Embaye, T., Turk, K., Kubo, M., Summons, R., et al. (2008). Lipid biomarker and phylogenetic analyses to reveal archaeal biodiversity and distribution in hypersaline microbial mat and underlying sediment. *Geobiology* 6, 394–410. doi:10.1111/j.1472-4669.2008.00165.x

Jankowski, B. (1981). *Die Geschichte der Sedimentation im Nördlinger Ries und Randecker Maar*. Bochum: Ruhr-Universität Bochum.

Jankowski, B. (1977). *Die postimpact-sedimente in der Forschungsbohrung nördlingen 1973*, 75. Munich: Geologica Bavarica, 21–36.

Jiang, K., Lin, C., Peng, L., Zhang, X., and Cai, C. (2019). Methyltrimethyltridecylchromans (MTTCs) in lacustrine sediments in the northern bohai bay basin, China. *Org. Geochem.* 133, 1–9. doi:10.1016/j.orggeochem.2019.03.003

Jiang, K., Lin, C., Zhang, X., Cai, C., Xiao, F., He, W., et al. (2018). Variations in abundance and distribution of methyltrimethyltridecylchromans (MTTCs) in sediments from saline lacustrine settings in Cenozoic lacustrine basins, China. *Org. Geochem.* 121, 58–67. doi:10.1016/j.orggeochem.2018.03.006

Jiang, L., Ding, W., and George, S. C. (2020). Late cretaceous–paleogene palaeoclimate reconstruction of the gippsland basin, SE Australia. *Palaeogeogr. Palaeoclimatol. Palaeoecol.* 556, 109885. doi:10.1016/j.palaeo.2020.109885

Kenig, F., Sinninghe Damsté, J. S., Frewin, N. L., Hayes, J., and De Leeuw, J. W. (1995). Molecular indicators for palaeoenvironmental change in a Messinian evaporitic sequence (Vena del Gesso, Italy). II: High-resolution variations in abundances and 13C contents of free and sulphur-bound carbon skeletons in a single marl bed. *Org. Geochem.* 23, 485–526. doi:10.1016/0146-6380(95)00049-k

Kodner, R. B., Pearson, A., Summons, R. E., and Knoll, A. H. (2008). Sterols in red and green algae: Quantification, phylogeny, and relevance for the interpretation of geologic steranes. *Geobiology* 6, 411–420. doi:10.1111/j.1472-4669.2008.00167.x

Koeberl, C., Milkereit, B., Overpeck, J. T., Scholz, C. A., Amoako, P. Y., Boamah, D., et al. (2007). An international and multidisciplinary drilling project into a young complex impact structure: The 2004 ICDP bosumtwi crater drilling project—an overview. *Meteorit. Planet. Sci.* 42, 483–511. doi:10.1111/j.1945-5100.2007.tb01057.x

Largeau, C., and Derenne, S. (1993). Relative efficiency of the selective preservation and degradation recondensation pathways in kerogen formation. Source and environment influence on their contributions to type I and II kerogens. *Org. Geochem.* 20, 611–615. doi:10.1016/0146-6380(93)90027-9

Littke, R., Urai, J. L., Uffmann, A. K., and Risvanis, F. (2012). Reflectance of dispersed vitrinite in Palaeozoic rocks with and without cleavage: Implications for burial and thermal history modeling in the Devonian of Rursee area, northern Rhenish Massif, Germany. *Int. J. Coal Geol.* 89, 41–50. doi:10.1016/j.coal.2011.07.006

Lowenstein, T. K., Jagniecki, E. A., Carroll, A. R., Smith, M. E., Renaut, R. W., and Owen, R. B. (2017). The Green River salt mystery: What was the source of the hyperalkaline lake waters? *Earth. Sci. Rev.* 173, 295–306. doi:10.1016/j.earscirev.2017.07.014

Mackenzie, A., Brassell, S., Eglinton, G., and Maxwell, J. (1982). Chemical fossils: The geological fate of steroids. *Science* 217, 491–504. doi:10.1126/science.217.4559.491

McGenity, T. J., and Sorokin, D. Y. (2010). *Handbook of hydrocarbon and lipid microbiology*. Cham: Springer, 665–680.Methanogens and methanogenesis in hypersaline environments

Melosh, H., and Ivanov, B. (1999). Impact crater collapse. *Annu. Rev. Earth Planet. Sci.* 27, 385–415. doi:10.1146/annurev.earth.27.1.385

Meyers, P. A. (1997). Organic geochemical proxies of paleoceanographic, paleolimnologic, and paleoclimatic processes. *Org. Geochem.* 27, 213–250. doi:10.1016/s0146-6380(97)00049-1

Mohriak, W., Mello, M., Dewey, J., and Maxwell, J. (1990). *Petroleum geology of the Campos basin, offshore Brazil*. London: Geological Society, 50, 119–141.

Montano, D., Gasparrini, M., Gerdes, A., Della Porta, G., and Albert, R. (2021). *In-situ* U-Pb dating of Ries Crater lacustrine carbonates (Miocene, South-West Germany): Implications for continental carbonate chronostratigraphy. *Earth Planet. Sci. Lett.* 568, 117011. doi:10.1016/j.epsl.2021.117011

Mujal, E., and Schoch, R. R. (2020). Middle Triassic (Ladinian) amphibian tracks from the Lower Keuper succession of southern Germany: Implications for temnospondyl locomotion and track preservation. *Palaeogeogr. Palaeoclimatol. Palaeoecol.* 543, 109625. doi:10.1016/j.palaeo.2020.109625

Noble, R. A., Alexander, R., Kagi, R. I., and Nox, J. K. (1986). Identification of some diterpenoid hydrocarbons in petroleum. *Org. Geochem.* 10, 825–829. doi:10.1016/s0146-6380(86)80019-5

Pagani, M., Freeman, K. H., and Arthur, M. A. (2000). Isotope analyses of molecular and total organic carbon from Miocene sediments. *Geochim. Cosmochim. Acta* 64, 37–49. doi:10.1016/s0016-7037(99)00151-9

Pawlowska, M. M., Butterfield, N. J., and Brocks, J. J. (2013). Lipid taphonomy in the Proterozoic and the effect of microbial mats on biomarker preservation. *Geology* 41 (2), 103–106. doi:10.1130/g33525.1

Pecoraino, G., D'Alessandro, W., and Inguaggiato, S. (2015). *The other side of the coin: Geochemistry of alkaline lakes in volcanic areas, volcanic lakes*. Berlin, Heidelberg: Springer, 219–237.

Pohl, J., Stoeffler, D., Gall, H., and Ernstson, K. (1977). *The Ries impact crater, Impact and explosion cratering: Planetary and terrestrial implications*. New York: Pergamon Press, 343–404.

Prinz, L., Zieger, L., Littke, R., McCann, T., Lokay, P., and Asmus, S. (2017). Syn- and post-depositional sand bodies in lignite–the role of coal analysis in their recognition. A study from the Frimmersdorf Seam, Garzweiler open-cast mine, western Germany. *Int. J. Coal Geol.* 179, 173–186. doi:10.1016/j.coal.2017.05.014

Riding, R. (1979). Origin and diagenesis of lacustrine algal bioherms at the margin of the Ries crater, Upper Miocene, southern Germany. *Sedimentology* 26, 645–680. doi:10.1111/j.1365-3091.1979.tb00936.x

Rohmer, M., Bouvier-Nave, P., and Ourisson, G. (1984). Distribution of hopanoid triterpenes in prokaryotes. *Microbiology* 130, 1137–1150. doi:10.1099/00221287-130-5-1137

Rothe, P., and Hoefs, J. (1977). Isotopen-geochemische untersuchungen an karbonaten der Ries-See-Sedimente der Forschungbohrung nördlingen 1973. *Geol. Bavarica* 75, 59–66.

Rowland, S. (1990). Production of acyclic isoprenoid hydrocarbons by laboratory maturation of methanogenic bacteria. *Org. Geochem.* 15, 9–16. doi:10.1016/0146-6380(90)90181-x

Rowland, S., and Robson, J. (1990). The widespread occurrence of highly branched acyclic $C_{20}$, $C_{25}$ and $C_{30}$ hydrocarbons in recent sediments and biota—A review. *Mar. Environ. Res.* 30, 191–216. doi:10.1016/0141-1136(90)90019-k

Rullkötter, J., Littke, R., and Schaefer, R. G. (1990). *Characterization of organic matter in sulfur-rich lacustrine sediments of Miocene age (Nördlinger Ries, southern Germany)*. Washington, DC: American Chemical Society.

Rullkötter, J., and Philip, P. (1981). Extended hopanes up to $C_{40}$ in Thornton bitumen. *Nature* 292 (5824), 616–618. doi:10.1038/292616a0

Salger, M. (1977). Clay minerals from the borehole Nördlingen 1973. *Geol. Bavarica* 75, 67–73.

Saraswati, P. K. (2015). *Time averaging and compositional averaging in biogenic carbonates: Implications for chemostratigraphy, chemostratigraphy*. Netherland: Elsevier, 93–101.

Schinteie, R., and Brocks, J. (2017). Paleoecology of neoproterozoic hypersaline environments: Biomarker evidence for haloarchaea, methanogens, and cyanobacteria. *Geobiology* 15, 641–663. doi:10.1111/gbi.12245

Schouten, S., Hartgers, W. A., Lòpez, J. F., Grimalt, J. O., and Sinninghe Damsté, J. S. (2001). A molecular isotopic study of 13C-enriched organic matter in evaporitic deposits: Recognition of CO2-limited ecosystems. *Org. Geochem.* 32, 277–286. doi:10.1016/s0146-6380(00)00177-7

Schouten, S., Özdirekcan, S., van der Meer, M. T., Blokker, P., Baas, M., Hayes, J. M., et al. (2008). Evidence for substantial intramolecular heterogeneity in the stable carbon isotopic composition of phytol in photoautotrophic organisms. *Org. Geochem.* 39 (1), 135–146. doi:10.1016/j.orggeochem.2007.09.002

Schwark, L., Vliex, M., and Schaeffer, P. (1998). Geochemical characterization of Malm zeta laminated carbonates from the franconian Alb, SW-Germany (II). *Org. Geochem.* 29, 1921–1952. doi:10.1016/s0146-6380(98)00192-2

Schwarzbauer, J., Littke, R., Meier, R., and Strauss, H. (2013). Stable carbon isotope ratios of aliphatic biomarkers in Late Palaeozoic coals. *Int. J. Coal Geol.* 107, 127–140. doi:10.1016/j.coal.2012.10.001

Schwarzbauer, J., Littke, R., and Weigelt, V. (2000). Identification of specific organic contaminants for estimating the contribution of the Elbe river to the pollution of the German Bight. *Org. Geochem.* 31, 1713–1731. doi:10.1016/s0146-6380(00)00076-0

Shanahan, T. M., Overpeck, J. T., Anchukaitis, K., Beck, J. W., Cole, J. E., Dettman, D. L., et al. (2009). Atlantic forcing of persistent drought in West Africa. *Science* 324, 377–380. doi:10.1126/science.1166352

Shanmugam, G. (1985). Significance of coniferous rain forests and related organic matter in generating commercial quantities of oil, Gippsland Basin, Australia. *AAPG Bull.* 69, 1241–1254.

Shiea, J., Brassell, S. C., and Ward, D. M. (1990). Mid-chain branched mono-and dimethyl alkanes in hot spring cyanobacterial mats: A direct biogenic source for branched alkanes in ancient sediments? *Org. Geochem.* 15, 223–231. doi:10.1016/0146-6380(90)90001-g

Simoneit, B. R., Grimalt, J., Wang, T., Cox, R., Hatcher, P. G., and Nissenbaum, A. (1986). Cyclic terpenoids of contemporary resinous plant detritus and of fossil woods, ambers and coals. *Org. Geochem.* 10, 877–889. doi:10.1016/s0146-6380(86)80025-0

Sinninghe Damsté, J. S., Kenig, F., Koopmans, M. P., Köster, J., Schouten, S., Hayes, J., et al. (1995). Evidence for gammacerane as an indicator of water column stratification. *Geochim. Cosmochim. Acta* 59, 1895–1900. doi:10.1016/0016-7037(95)00073-9

Southgate, P., Lambert, I., Donnelly, T., Henry, R., Etminan, H., and Weste, G. (1989). Depositional environments and diagenesis in lake parakeelya: A cambrian alkaline playa from the Officer Basin, south Australia. *Sedimentology* 36, 1091–1112. doi:10.1111/j.1365-3091.1989.tb01544.x

Stock, A. T., Littke, R., Luecke, A., Zieger, L., and Thielemann, T. (2016). Miocene depositional environment and climate in western Europe: The lignite deposits of the Lower Rhine Basin, Germany. *Int. J. Coal Geol.* 157, 2–18. doi:10.1016/j.coal.2015.06.009

Stöffler, D., Artemieva, N. A., Wünnemann, K., Reimold, W. U., Jacob, J., Hansen, B. K., et al. (2013). Ries crater and suevite revisited—observations and modeling Part I: Observations. *Meteorit. Planet. Sci.* 48, 515–589. doi:10.1111/maps.12086

Stöffler, D., and Wu, R. (1977). Research drilling Nördlingen 1973 (Ries): Composition and texture of polymict impact breccias. *Geol. Bavarica* 75, 163–189.

Stüeken, E. E., Buick, R., and Schauer, A. (2015). Nitrogen isotope evidence for alkaline lakes on late Archean continents. *Earth Planet. Sci. Lett.* 411, 1–10. doi:10.1016/j.epsl.2014.11.037

Stüeken, E. E., Kipp, M. A., Koehler, M. C., and Buick, R. (2016). The evolution of Earth's biogeochemical nitrogen cycle. *Earth. Sci. Rev.* 160, 220–239. doi:10.1016/j.earscirev.2016.07.007

Stüeken, E. E., Martinez, A., Love, G., Olsen, P. E., Bates, S., and Lyons, T. W. (2019). Effects of pH on redox proxies in a Jurassic rift lake: Implications for interpreting environmental records in deep time. *Geochim. Cosmochim. Acta* 252, 240–267. doi:10.1016/j.gca.2019.03.014

Stüeken, E. E., Tino, C., Arp, G., Jung, D., and Lyons, T. W. (2020). Nitrogen isotope ratios trace high-pH conditions in a terrestrial Mars analog site. *Sci. Adv.* 6, eaay3440. doi:10.1126/sciadv.aay3440

Sturm, S., Kenkmann, T., Willmes, M., Pösges, G., and Hiesinger, H. (2015). The distribution of megablocks in the Ries crater, Germany: Remote sensing, field investigation, and statistical analyses. *Meteorit. Planet. Sci.* 50, 141–171. doi:10.1111/maps.12408

Summons, R. E., Franzmann, P. D., and Nichols, P. D. (1998). Carbon isotopic fractionation associated with methylotrophic methanogenesis. *Org. Geochem.* 28, 465–475. doi:10.1016/s0146-6380(98)00011-4

Taylor, G. H., Teichmüller, M., Davis, A., Diessel, C., Littke, R., and Robert, P. (1998). *Organic petrology*. Berlin: Gebrüder Borntraeger.

ten Haven, H., De Leeuw, J., Rullkötter, J., and Sinninghe Damsté, J. S. (1987). Restricted utility of the pristane/phytane ratio as a palaeoenvironmental indicator. *Nature* 330, 641–643. doi:10.1038/330641a0

ten Haven, H. L., Rohmer, M., Rullk¨otter, J., and Bisseret, P. (1989). Tetrahymanol, the most likely precursor of gammacerane, occurs ubiquitously in marine sediments. *Geochim. Cosmochim. Acta* 53, 3073–3079. doi:10.1016/0016-7037(89)90186-5

Trendel, J., Lohmann, F., Kintzinger, J., Albrecht, P., Chiarone, A., Riche, C., et al. (1989). Identification of des-A-triterpenoid hydrocarbons occurring in surface sediments. *Tetrahedron* 45, 4457–4470. doi:10.1016/s0040-4020(01)89081-5

Tulipani, S., Grice, K., Greenwood, P. F., Schwark, L., Boettcher, M. E., Summons, R. E., et al. (2015). Molecular proxies as indicators of freshwater incursion-driven salinity stratification. *Chem. Geol.* 409, 61–68. doi:10.1016/j.chemgeo.2015.05.009

van Aarssen, B. G., Alexander, R., and Kagi, R. I. (2000). Higher plant biomarkers reflect palaeovegetation changes during Jurassic times. *Geochim. Cosmochim. Acta* 64, 1417–1424. doi:10.1016/s0016-7037(99)00432-9

Volkman, J. K. (1986). A review of sterol markers for marine and terrigenous organic matter. *Org. Geochem.* 9, 83–99. doi:10.1016/0146-6380(86)90089-6

Volkman, J. K., Zhang, Z., Xie, X., Qin, J., and Borjigin, T. (2015). Biomarker evidence for *Botryococcus* and a methane cycle in the Eocene Huadian oil shale, NE China. *Org. Geochem.* 78, 121–134. doi:10.1016/j.orggeochem.2014.11.002

Wang, L., Song, Z., Yin, Q., and George, S. C. (2011). Paleosalinity significance of occurrence and distribution of methyltrimethyltridecyl chromans in the upper cretaceous nenjiang formation, songliao basin, China. *Org. Geochem.* 42, 1411–1419. doi:10.1016/j.orggeochem.2011.08.012

Wang, T., Cao, J., Jin, J., Xia, L., Xiang, B., Ma, W., et al. (2021). Spatiotemporal evolution of a late paleozoic alkaline lake in the Junggar Basin, China. *Mar. Pet. Geol.* 124, 104799. doi:10.1016/j.marpetgeo.2020.104799

Warren, J. K. (2016). *Evaporites: A geological compendium*. Heidelberg: Springer.

Wen, Z., Ruiyong, W., Radke, M., Qingyu, W., Guoying, S., and Zhili, L. (2000). Retene in pyrolysates of algal and bacterial organic matter. *Org. Geochem.* 31, 757–762. doi:10.1016/s0146-6380(00)00064-4

Wilkin, R. T., Barnes, H. L., and Brantley, S. L. (1996). The size distribution of framboidal pyrite in modern sediments: An indicator of redox conditions. *Geochim. Cosmochim. Acta* 60 (20), 3897–3912. doi:10.1016/0016-7037(96)00209-8

Wilms, R., Sass, H., Köpke, B., Cypionka, H., and Engelen, B. (2007). Methane and sulfate profiles within the subsurface of a tidal flat are reflected by the distribution of sulfate-reducing bacteria and methanogenic archaea. *FEMS Microbiol. Ecol.* 59, 611–621. doi:10.1111/j.1574-6941.2006.00225.x

Wolf, M., and Füchtbauer, H. (1976). *Die karbonatische Randfazies der tertiären Süßwasserseen des Nördlinger Ries und des Steinheimer Beckens*. Stuttgart, Germany: Schweizerbart, 3–53. Geol. Jb.

Xia, L., Cao, J., Hu, W., Zhi, D., Tang, Y., Li, E., et al. (2021). Coupling of paleoenvironment and biogeochemistry of deep-time alkaline lakes: A lipid biomarker perspective. *Earth. Sci. Rev.* 213, 103499. doi:10.1016/j.earscirev.2020.103499

Yang, J., Yi, C., Du, Y., Zhang, Z., and Yan, J. (2015). Geochemical significance of the Paleogene soda-deposits bearing strata in biyang depression, henan province. *Sci. China Earth Sci.* 58, 129–137. doi:10.1007/s11430-014-4963-8

Yang, S., and Horsfield, B. (2020). Critical review of the uncertainty of Tmax in revealing the thermal maturity of organic matter in sedimentary rocks. *Int. J. Coal Geol.* 225, 103500. doi:10.1016/j.coal.2020.103500

Zeng, L., Ruge, D. B., Berger, G., Heck, K., Hölzl, S., Reimer, A., et al. (2021). Sedimentological and carbonate isotope signatures to identify fluvial processes and catchment changes in a supposed impact ejecta-dammed lake (Miocene, Germany). *Sedimentology* 68, 2965–2995. doi:10.1111/sed.12888

Zhang, Y., Jiang, A., Sun, Y., Xie, L., and Chai, P. (2012). Stable carbon isotope compositions of isoprenoid chromans in Cenozoic saline lacustrine source rocks from the Western Qaidam Basin, NW China: Source implications. *Chin. Sci. Bull.* 57, 1013–1023. doi:10.1007/s11434-011-4899-8

Zhao, Z., Hou, D., Cheng, X., Xu, H., Ma, C., Zhou, X., et al. (2021). Geochemical and palynological characteristics of the Paleogene source rocks in the Northeastern Laizhouwan Sag, Bohai Bay Basin, China: Hydrocarbon potential, depositional environment, and factors controlling organic matter enrichment. *Mar. Pet. Geol.* 124, 104792. doi:10.1016/j.marpetgeo.2020.104792

Zhao, Z., Littke, R., Zieger, L., Hou, D., and Felix, F. (2020). Depositional environment, thermal maturity and shale oil potential of the Cretaceous Qingshankou Formation in the eastern Changling Sag, Songliao Basin, China: An integrated organic and inorganic geochemistry approach. *Int. J. Coal Geol.* 232, 103621. doi:10.1016/j.coal.2020.103621